
The Shapes and Stability of Captive Rotating Drops

R. A. Brown and L. E. Scriven

Phil. Trans. R. Soc. Lond. A 1980 **297**, 51-79

doi: 10.1098/rsta.1980.0204

Email alerting service

Receive free email alerts when new articles cite this article - sign up in the box at the top right-hand corner of the article or click [here](#)

To subscribe to *Phil. Trans. R. Soc. Lond. A* go to: <http://rsta.royalsocietypublishing.org/subscriptions>

THE SHAPES AND STABILITY OF CAPTIVE ROTATING DROPS

BY R. A. BROWN† AND L. E. SCRIVEN

*Department of Chemical Engineering and Materials Science, University of Minnesota,
Minneapolis, MN 55455, U.S.A.*

*(Communicated by Sir James Lighthill, F.R.S. – Received 19 February 1979 –
Revised 14 September 1979)*

CONTENTS

	PAGE
1. INTRODUCTION	52
2. GYROSTATIC EQUILIBRIUM DROP SHAPE	55
3. STABILITY AND SHAPE BIFURCATION	56
4. SPECIAL CASE: CYLINDRICAL DROP	59
(a) Bifurcations to axisymmetric drop shapes	60
(b) Bifurcations to nonaxisymmetric drop shapes	62
5. COMPUTER-AIDED ANALYSIS	63
(a) Drop shape	63
(b) Stability and bifurcation	65
6. RESULTS	68
(a) Drops having the volume of a cylinder	70
(b) Drops not having the volume of a cylinder	73
7. DISCUSSION	76
REFERENCES	78

Computer-aided means are presented for constructing entire families of solutions to Young and Laplace's nonlinear partial differential equation of capillarity, with the enclosed volume prescribed, and of determining the stability of the solutions and bifurcations between families having different three-dimensional symmetry properties; equivalently, these are means for surveying the topography of corresponding energy surfaces in especially convenient finite-dimensional function spaces spanned by so-called finite element bases in which both the solutions and variations of them are represented. The means are a finite element algorithm employing Newton iteration and, for the stability and bifurcation eigenproblem, a block-Lanczos method.

The algorithm is applied to gyrostatic liquid drops of fixed volume held captive between two co-rotating, parallel, concentric faces or contact circles and acted on by surface tension and centrifugal force. The results for the special case of captive cylindrical drops compare well with published and new results of conventional stability and bifurcation analysis. Axisymmetric drop shapes that evolve from rest shapes of constant mean curvature are found to form a one-parameter family in rotational Bond number

† Present address: Department of Chemical Engineering, Massachusetts Institute of Technology, Cambridge, MA 02139, U.S.A.

$\Sigma \equiv \Omega^2 R^3 \Delta \rho / 8\sigma$. Bifurcating axisymmetric and three-dimensional families are calculated. The limit of stability is found to lie in the family of simplest axisymmetric drops, except in the case of very fat ones, which exchange stability with C-shaped drops, a remarkable fact.

Implications for the experiments of Plateau, Carruthers & Grasso, and others are discussed.

1. INTRODUCTION

Young (1805) and Laplace (1805) pioneered the analysis of equilibrium shapes of menisci – fluid interfaces with surface tension – between pairs of immiscible fluids. Most of the theory has been directed toward integration of the differential equation of shapes of menisci, the well-known Young–Laplace equation. Solutions are candidate equilibrium shapes, but whether or not they are physically realizable is a more difficult issue of stability, which is not as well studied.

The forces in and on an interface between static fluids or between rigidly rotating fluids are conservative. Consequently, a potential energy of such a system can be defined and the Young–Laplace equation is the Euler–Lagrange condition for an extremum of that potential, besides being a statement of the local balance of forces on the interface. The force and energy formulations are of course fully equivalent, but for present purposes the latter is convenient because it leads to the mathematical machinery of the calculus of variations for studying both the equilibrium meniscus shapes and their stability. This is an old approach (Rayleigh 1879; Howe 1887) but so far as we know has been implemented only for translationally symmetric and rotationally symmetric menisci (see, for example, Gillette & Dyson 1971; Huh 1969; Pitts 1973, 1974, 1976, Majumdar & Michael 1976; Coriell *et al.* 1977). For such menisci the Young–Laplace equation reduces to a nonlinear *ordinary* differential equation, solutions of which are only rarely simple combinations of tabulated functions. Generally, the equation must be integrated numerically for meniscus shape.

This is true of sessile and pendent drop shapes. Nevertheless Pitts (1974, 1975) and others (Majumdar & Michael 1976; Michael & Williams 1976, 1977) obtained, by energy methods, mathematical expressions in closed form for the condition of neutral stability of translationally symmetric and of rotationally symmetric sessile and pendent drops. It appears, however, that these methods do not, or at least do not easily, extend to three-dimensional menisci.

In this paper we describe a computer-aided means of constructing solutions to the full Young–Laplace equation and to similar nonlinear partial differential equations, and simultaneously determining the stability of the solutions so constructed. The stability determined is with respect to all small disturbances that can be represented in the same finite-dimensional function basis from which the solution is built. The solution satisfies the Young–Laplace equation only in the Galerkin sense (Finlayson 1972) and thus is approximate, strictly speaking, although it can in principle be refined as desired, save for the practical limitation imposed by computational cost. The framework we use is the subdomain scheme known as the finite element method, in which approximations to solutions are built out of many low-order polynomials, each of which is non-zero only in a small subdomain of the entire problem domain. On this framework we develop an essentially numerical algorithm for calculating equilibrium shapes and stability of three-dimensional menisci. The algorithm is presented in § 5. Earlier, we applied finite element analysis to the calculations of equilibrium interface shapes without regard to their stability (Orr *et al.* 1975; Brown *et al.* 1980; Brown 1979).

In a progression of meniscus shapes, the occurrence of neutral stability corresponds to a point of bifurcation where two or more equilibrium shape families join, as Majumdar & Michael (1976; see also Michael & Williams 1976, 1977) point out in connection with the energy approach to stability. Generally, the complete representation of a meniscus shape requires an infinite-dimensional, complete function basis, and thus the space in which to picture fully the potential energy surface of a meniscus system is infinite-dimensional. In figure 1 such a space is, in effect, projected

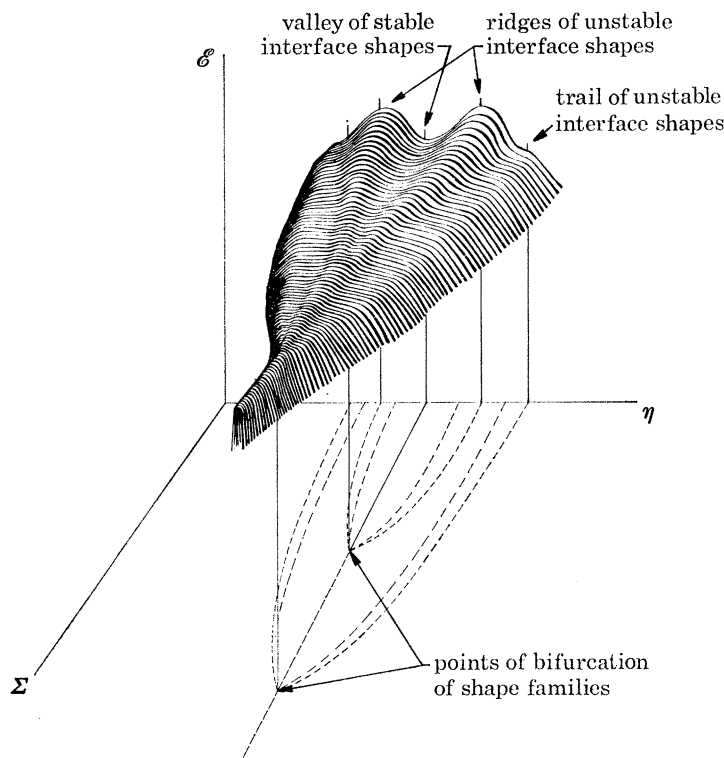


FIGURE 1. Potential energy \mathcal{E} in a region of bifurcation points between families of equilibrium interface shapes. Shown is a projection of the multidimensional potential energy surface onto a single, key basis function η together with a single parameter Σ representing a ratio of forces at the interface.

into a three-dimensional subspace consisting of potential energy \mathcal{E} , a parameter Σ (which in the next section is identified as the rotational Bond number of rotating drops), and the coefficient of a single, key basis function. In figure 1, then, a local minimum in the energy surface where it is cut by a plane of constant Σ corresponds to a stable equilibrium shape, whereas other local extrema in the same intersection correspond to unstable equilibrium shapes. A shape family is a sequence of shapes that is continuous in the parameter Σ . A stable family is represented by a valley-line; an unstable family, by a ridge-line. When a shape is neutrally stable there are certain infinitesimal perturbations of it that leave the energy of the system unchanged to second order. If these perturbations can be expressed in terms of the single basis function of figure 1, then neutral stability (ordinarily) corresponds to a point where a valley-line meets a ridge-line. Such a point is a bifurcation point. Thompson & Hunt (1973, 1975) detail the bifurcations topologically possible for conservative systems with potential energy defined by a finite number of coordinates or, as is done here, accurately approximated in a finite-dimensional basis.

Our numerical algorithm exploits the connection between neutral stability and solution branching to locate bifurcation points by finite element analysis. Moreover, the shape perturbation that causes neutral stability is determined and used to calculate nearby shapes in the bifurcating shape family. Thus identified, this shape family can be tracked across the energy landscape until it in turn bifurcates, or simply terminates, or merely becomes uninteresting. In this way we can trace out the entire family tree of equilibrium drop shapes, stable and unstable, which, with respect to a parameter Σ , evolve continuously from one known equilibrium drop shape. This approach also yields family trees of solutions of other nonlinear partial differential equations, and so should find applications outside the subject of capillarity to which this paper is addressed.

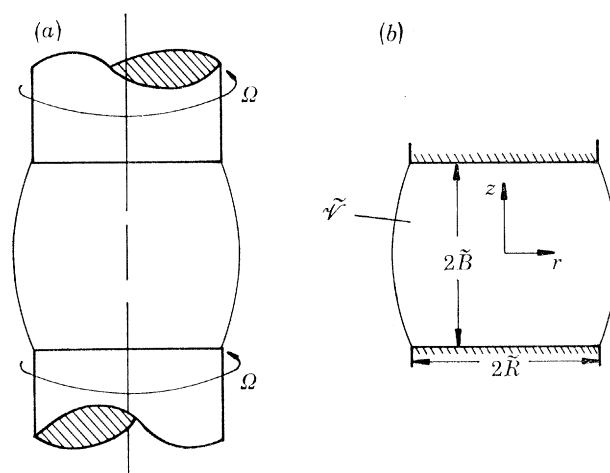


FIGURE 2. A rotating captive liquid drop (a) of volume \mathcal{V} with its dimensions (b).

The problem solved here is representative: the shape and stability of a rigidly rotating liquid drop held captive, in the absence of gravity, between two parallel, circular, solid faces co-rotating about their common axis as shown in figure 2. This problem is practically important because of its relation to the float-zone process for refining molten materials and producing single crystals (Carruthers 1975; Carruthers & Grasso 1972 *a, b*; Coriell *et al.* 1977). In the absence of gravity, a perfectly cylindrical captive drop, or liquid column, of the same radius as the solid faces is an equilibrium drop configuration, though its stability is another matter. The stability of cylindrical captive drops with respect to axisymmetric and to certain non-axisymmetric shapes was analysed by Hardy & Coriell (1974), and Fowle *et al.* (1976) also conducted experiments to elucidate the instabilities of rotating cylindrical drops, but their results differed and led to conflicting interpretations. These are discussed in §7 in the light of the theoretical results found with the new algorithm.

Basic elements of the algorithm can be illustrated with the perfectly cylindrical captive drop. The stability and bifurcation of this special shape family are tractable by conventional techniques, the results of which are summarized in §4 and used to test the algorithm before it is applied to more general cases in §5.

Throughout this paper the Earth's gravitational potential is considered to be either absent or insignificant in its effect. Although this may be justified for sufficiently small drops of great enough surface tension, the shape and stability of centimetre-size drops with moderate surface tension is influenced by gravity. Gravity in any amount in an axial direction disrupts the reflective symmetry of drops about their equatorial planes. No doubt the topography of the energy surfaces of

equilibrium solutions is altered in amounts characterized by the gravitational Bond number, $G \equiv gR^2\Delta\rho/\sigma$, though these matters are not considered here. Coriell *et al.* (1977) and Coriell & Cordes (1977) computed the shapes of axisymmetric captive drops influenced by gravity and determined the stability of these shapes with respect to both axisymmetric and asymmetric shape perturbations. Their algorithm is based on Huh's (1969) shooting method for calculating shape and stability of axisymmetric menisci and cannot easily be generalized to study truly three-dimensional interfaces.

2. GYROSTATIC EQUILIBRIUM DROP SHAPE

Consider a drop of volume $\tilde{\mathcal{V}}$ trapped in the gap of length $2\tilde{B}$ between two coaxial solid faces of radius \tilde{R} , both of which are rotating at angular velocity Ω . The liquid completely wets the two faces and the meniscus joins the edge of each face: thus the meniscus terminates in circular contact lines of radius \tilde{R} at which a wide range of contact angles is admitted here even though there may be certain bounds on contact angle in reality. The surrounding fluid exerts uniform pressure and negligible viscous drag on the rotating liquid.

In cylindrical polar coordinates the shape of the drop is conveniently $\tilde{r} = \tilde{f}(\tilde{z}, \theta)$. Any radial function $\tilde{f}(\tilde{z}, \theta)$ describes an equilibrium shape if (1) it gives an extremum in Helmholtz's 'effective potential,'

$$\tilde{\mathcal{E}} = \int_0^\pi \int_{-\tilde{B}}^{\tilde{B}} [(\sigma\sqrt{\tilde{f}^2 + \tilde{f}_z^2 \tilde{f}_\theta^2 + \tilde{f}_\theta^3}) - \frac{1}{8}\Delta\rho\Omega^2\tilde{f}^4] d\tilde{z} d\theta, \quad (2.1)$$

(2) it enclosed the prescribed volume $\tilde{\mathcal{V}}$,

$$\tilde{\mathcal{V}} = \frac{1}{2} \int_0^\pi \int_{-\tilde{B}}^{\tilde{B}} \tilde{f}^2 d\tilde{z} d\theta, \quad (2.2)$$

and (3) it satisfies the wetting conditions,

$$\tilde{f}(-\tilde{B}, \theta) = \tilde{f}(\tilde{B}, \theta) = \tilde{R}, \quad 0 \leq \theta \leq \pi. \quad (2.3)$$

In (2.1) σ is the surface tension and $\Delta\rho$ is the density difference between the rotating liquid and the surrounding fluid. The drop shape is presumed to have a plane of reflective symmetry that passes through the axis of rotation. One sheet of this plane is taken as the datum $\theta = 0$; thus

$$\tilde{f}_\theta(\tilde{z}, 0) = \tilde{f}_\theta(\tilde{z}, \pi) = 0, \quad -\tilde{B} \leq \tilde{z} \leq \tilde{B}. \quad (2.4)$$

It is convenient to use the radius \tilde{R} as the length scale and to employ dimensionless variables:

$$\tilde{z} \equiv z/\tilde{R}, \quad f \equiv \tilde{f}/\tilde{R}, \quad (2.5)$$

$$\mathcal{E} \equiv \tilde{\mathcal{E}}/\sigma\tilde{R}^2 = \int_0^\pi \int_{-B}^B [\mathcal{S}(f, f_z, f_\theta) - \Sigma f^4] dz d\theta, \quad (2.6)$$

$$\mathcal{V} \equiv \tilde{\mathcal{V}}/\tilde{R}^3 = \frac{1}{2} \int_0^\pi \int_{-B}^B f^2 dz d\theta, \quad (2.7)$$

where $\mathcal{S}(f, f_\theta, f_z)$ – henceforth abbreviated as \mathcal{S} – is defined in terms of the dimensionless element of surface area:

$$d\mathcal{A} \equiv \mathcal{S} dz d\theta \equiv \sqrt{(f^2 + f_z^2 f_\theta^2 + f_\theta^3)} dz d\theta. \quad (2.8)$$

The dimensionless measure of the square of angular velocity is known as the rotational Bond number Σ :

$$\Sigma \equiv \tilde{R}^3\Omega^2\Delta\rho/8\sigma. \quad (2.9)$$

Positive values correspond to drops of more dense liquid rotating in contact with less dense outer fluid; negative values correspond to the converse, i.e. captive rotating bubbles. In dimensionless form the boundary conditions (2.4) and (2.5) are

$$\left. \begin{aligned} f(-B, \theta) = f(B, \theta) = 1, \quad 0 \leq \theta \leq \pi, \\ f_\theta(z, 0) = f_\theta(z, \pi) = 0, \quad -B \leq z \leq B. \end{aligned} \right\} \quad (2.10)$$

Gyrostatic equilibrium shapes of a captive drop of volume \mathcal{V} are given by those functions f that cause the first variation of the augmented effective potential to vanish:

$$\mathcal{H} \equiv \mathcal{E} - K\mathcal{V} = \int_0^\pi \int_{-B}^B (\mathcal{S} - \Sigma f^4 - Kf^2) dz d\theta, \quad (2.11)$$

where K is the Lagrange multiplier introduced with the volume constraint (2.7). The first variation with respect to all shapes that satisfy the wetting condition is

$$\begin{aligned} \delta\mathcal{H} &= \int_0^\pi \int_{-B}^B (\mathcal{S}_f \eta + \mathcal{S}_{f_z} \eta_z + \mathcal{S}_{f_\theta} \eta_\theta - 4\Sigma f^3 \eta - 2Kf\eta) dz d\theta \\ &= \int_0^\pi \int_{-B}^B \left\{ \frac{f\eta + ff_z \eta_z + f^2 f_z \eta_z + f_\theta \eta_\theta}{\sqrt{(f^2 + f^2 f_z^2 + f_\theta^2)}} - 4\Sigma f^3 \eta - 2Kf\eta \right\} dz d\theta = 0, \end{aligned} \quad (2.12)$$

where $\eta(z, \theta)$ is the variation of the equilibrium drop shape $f(z, \theta)$. This is equivalent to the Euler–Lagrange equation (Courant & Hilbert 1953, p. 183)

$$\begin{aligned} 4\Sigma f^2 + 2K &= \frac{1}{f} \left(\mathcal{S}_f - \frac{\partial}{\partial z} \mathcal{S}_{f_z} - \frac{\partial}{\partial \theta} \mathcal{S}_{f_\theta} \right), \\ 4\Sigma f^2 + 2K &= \frac{2f_\theta f_z f_{\theta z} + (f^2 + f_\theta^2) f_{zz} - (1 + f_z^2) f_{\theta\theta} + f(1 + f_z^2 + 2f_\theta^2/f^2)}{f^2 [1 + f_z^2 + f_\theta^2/f^2]^{\frac{3}{2}}}. \end{aligned} \quad (2.13)$$

This is precisely the Young–Laplace equation for meniscus shape. The quasi-linear differential operator on the right is the local mean curvature. The left-hand side is the (dimensionless) pressure difference across the meniscus. K is related to the datum difference Δp_0 which would occur at the axis of rotation if the meniscus reached the axis:

$$K \equiv \tilde{R} \Delta p_0 / 2\sigma, \quad (2.14)$$

and $4\Sigma f^2$ is proportional to the additional difference caused at $\tilde{r} = \tilde{f}$ by the rigid rotation. The product $-K\mathcal{V}$ in the augmented effective potential \mathcal{H} represents the pressure energy of the liquid in the drop.

3. STABILITY AND SHAPE BIFURCATION

Gyrostatic equilibrium at a prescribed angular velocity of rotation is stable if the effective potential $\mathcal{H}(f; \Sigma, \mathcal{V})$ is a local minimum with respect to all admissible infinitesimal perturbations of drop shape, as has long been known (cf. Lamb 1932; Lyttleton 1953). Here the admissible perturbations are those that preserve the volume of the drop and leave the wetting lines fixed on the edges of the faces. If the perturbations are $\eta(z, \theta)$, the condition for a minimum is that the second variation of \mathcal{H} about the equilibrium shape $f(z, \theta)$ be positive:

$$\begin{aligned} \delta^2 \mathcal{H} &= \int_0^\pi \int_{-B}^B (\mathcal{S}_{ff} \eta^2 + 2\mathcal{S}_{ff_\theta} \eta \eta_\theta + 2\mathcal{S}_{ff_z} \eta \eta_z + 2\mathcal{S}_{f_z f_\theta} \eta_\theta \eta_z \\ &\quad + \mathcal{S}_{f_z f_z} \eta_z^2 + \mathcal{S}_{f_\theta f_\theta} \eta_\theta^2 - 12f^2 \eta^2 - 2K\eta^2) dz d\theta > 0, \end{aligned} \quad (3.1)$$

while the constraints on $\eta(z, \theta)$ are

$$\delta \mathcal{V}(f, \eta) = \int_0^\pi \int_{-B}^B f(z, \theta) \eta(z, \theta) dz d\theta = 0, \quad (3.2)$$

$$\eta(-B, \theta) = \eta(B, \theta) = 0, \quad 0 \leq \theta \leq \pi. \quad (3.3)$$

These equations suggest that all directions around an equilibrium point on the potential energy surface indicated in figure 1 must be searched to find out if the point is a minimum. In fact it is necessary to check only in the principal directions of the surface, $\eta_i(z, \theta)$, for the signs of the second derivatives λ_i . Inequality (3.1) can be rearranged into a minimization problem,

$$\lambda_i = \min_{\eta_i(z, \theta)} \frac{\delta^2 \mathcal{H}(f, \eta; \Sigma, \mathcal{V})}{\langle \eta_i, \eta_i \rangle}, \quad (3.4)$$

over all perturbations that satisfy the requirements

$$\langle \eta_i, f \rangle = 0, \quad \langle \eta_i, \eta_j \rangle = 0, \quad j < i, \quad (3.5)$$

where brackets denote the inner product

$$\langle g, h \rangle = \int_0^\pi \int_{-B}^B g(z, \theta) h(z, \theta) dz d\theta. \quad (3.6)$$

The potential energy surface is locally concave toward higher energy and the equilibrium drop shape is stable if and only if all of the energy eigenvalues at the equilibrium point are positive, i.e.

$$\text{stability: } \lambda_i > 0, \quad i = 1, 2, \dots \quad (3.7)$$

Neutral stability is defined as the case in which one of the eigenvalues first reaches zero, in other words, when along a shape family the potential energy surface develops a flat point.

The Rayleigh quotient formulation (3.4) is fully equivalent to the following eigenproblem, which is more useful for the analytical purposes in §4:

$$\mathcal{L} \begin{bmatrix} \eta(z, \theta) \\ \beta \end{bmatrix} \equiv \begin{bmatrix} f\mathcal{L}(\eta) - 8\Sigma f^2 & -2f \\ \int_0^\pi \int_{-B}^B f(z, \theta) \eta(z, \theta) dz d\theta & 0 \end{bmatrix} \begin{bmatrix} \eta(z, \theta) \\ \beta \end{bmatrix} = \lambda \begin{bmatrix} \eta(z, \theta) \\ 0 \end{bmatrix}, \quad (3.8)$$

where the linear differential operator is defined by

$$\begin{aligned} \mathcal{L}(\eta) \equiv & \frac{1}{f} \left[\mathcal{S}_{ff} \eta + \mathcal{S}_{ffz} \eta_z + \mathcal{S}_{ff\theta} \eta_\theta - \frac{\partial}{\partial z} (\mathcal{S}_{ffz} \eta + \mathcal{S}_{fz f_\theta} \eta_\theta + \mathcal{S}_{fz f_z} \eta_z) \right. \\ & \left. - \frac{\partial}{\partial \theta} (\mathcal{S}_{ff\theta} \eta + \mathcal{S}_{fz f_\theta} \eta_z + \mathcal{S}_{f_\theta f_\theta} \eta) + \frac{\eta}{f} \left(\frac{\partial}{\partial z} \mathcal{S}_{f_\theta} + \frac{\partial}{\partial \theta} \mathcal{S}_{f_\theta} - \mathcal{S}_f \right) \right] \end{aligned} \quad (3.9)$$

and the eigenfunctions $\eta(z, \theta)$ satisfy (3.3). β is a Lagrange multiplier introduced to satisfy the volume constraint (3.2). The eigenfunction(s) belonging to a vanishing eigenvalue gives the direction(s) in which the potential energy surface is flat (to second order). Now we show that in this direction a second shape family branches off, or bifurcates, from the first at the flat point of neutral stability, as indicated in figure 1. The stability of both families beyond their bifurcation depends on the local topography of the energy surface.

Direction on the energy surface is a matter of the shape and in particular of the symmetry of captive drops of a given family. To find the unknown shape family bifurcating from a known

family $(f^{(0)}(z, \theta), K^{(0)})$ at a point of neutral stability we employ the power-series method (Millman & Keller 1969) to write the neighbouring shapes of the new family as a one-parameter perturbation class:

$$\left. \begin{aligned} f(z, \theta; \epsilon) &= f^{(0)}(z, \theta) + \epsilon f^{\hat{}}(z, \theta; \epsilon), \\ K(\epsilon) &= K^{(0)} + \epsilon \hat{K}(\epsilon). \end{aligned} \right\} \quad (3.10)$$

The parameter ϵ is a measure of the departure of a new shape from the neutrally stable shape of the known family, and is defined shortly. The perturbed shape and curvature, f and K , respectively, must obey the Young–Laplace equation (2.13), as do also $f^{(0)}$ and $K^{(0)}$; hence the shape perturbation function $f^{\hat{}}$ and curvature perturbation parameter \hat{K} must satisfy

$$\frac{1}{f^{\hat{}}} \left[\mathcal{L}_f - \frac{\partial}{\partial z} \mathcal{L}_{f_z} - \frac{\partial}{\partial \theta} \mathcal{L}_{f_\theta} \right]_{f=f^{\hat{}}} - \frac{1}{f^{(0)}} \left[\mathcal{L}_f - \frac{\partial}{\partial z} \mathcal{L}_{f_z} - \frac{\partial}{\partial \theta} \mathcal{L}_{f_\theta} \right]_{f=f^{(0)}} = 8\epsilon \Sigma f^{(0)} f^{\hat{}} + 4\epsilon^2 f^{\hat{2}} + 2\epsilon \hat{K}, \quad (3.11)$$

with the volume constraint

$$\int_0^\pi \int_{-B}^B (f^{(0)} + \epsilon f^{\hat{}})^2 dz d\theta = \mathcal{V} \quad (3.12)$$

and the boundary conditions

$$\left. \begin{aligned} f^{\hat{}}(\theta, -B) &= f^{\hat{}}(\theta, B) = 0, & 0 \leq \theta \leq \pi, \\ f^{\hat{}}_\theta(0, z) &= f^{\hat{}}_\theta(\pi, z) = 0, & -B \leq z \leq B. \end{aligned} \right\} \quad (3.13)$$

Following Millman & Keller (1969) we adopt the expansions

$$\begin{bmatrix} f^{\hat{}}(z, \theta; \epsilon) \\ K(\epsilon) \\ \Sigma(\epsilon) \end{bmatrix} = \sum_{n=0}^{\infty} \frac{\epsilon^n}{n!} \begin{bmatrix} f^{(n+1)}(z, \theta) \\ K^{(n+1)} \\ \Sigma^{(n)} \end{bmatrix}, \quad (3.14)$$

where the amplitude parameter is defined as an integral weighted difference between drop shapes:

$$\epsilon \equiv \langle f^{(1)}, f - f^{(0)} \rangle, \quad (3.15)$$

Substituted in (3.11)–(3.13) the expansions generate a set of linear partial differential equations with variable coefficients. Although these problems in principle can be solved sequentially they are, except in the special case of a cylindrical drop treated in the next section, quite formidable past the one that is first-order in ϵ . But this first-order problem makes clear the relation between bifurcation and neutral stability, as follows.

The first-order problem is

$$\mathcal{L} \begin{bmatrix} f^{(1)} \\ K^{(1)} \end{bmatrix} \equiv \begin{bmatrix} f^{(0)} \mathcal{L}(\) - 8\Sigma^{(0)} f^{(0)2} & -2f^{(0)} \\ \int_0^\pi \int_{-B}^B f^{(0)}(\) dz d\theta & 0 \end{bmatrix} \begin{bmatrix} f^{(1)} \\ K^{(1)} \end{bmatrix} = \begin{bmatrix} 0 \\ 0 \end{bmatrix}, \quad (3.16)$$

$$f^{(1)}(-B, \theta) = f^{(1)}(B, \theta) = 0, \quad 0 \leq \theta \leq \pi,$$

$$f^{(1)}_\theta(z, 0) = f^{(1)}_\theta(z, \pi) = 0, \quad -B \leq z \leq B.$$

where $\mathcal{L}(\)$ is the operator defined at (3.9) but with f replaced by $f^{(0)}$. Whereas the eigenproblem (3.8) describes the stability or instability of an equilibrium drop shape at rotational Bond number Σ , the problem (3.16) gives the values of $\Sigma = \Sigma^{(0)}$ at which new drop shapes bifurcate from the known shape $f(z, \theta; \Sigma, \mathcal{V})$. The bifurcation problem (3.16) is identical to (3.8) for a neutrally

stable perturbation ($\lambda_i = 0$). The neutrally stable perturbation $\eta_i(z, \theta)$ to the equilibrium interface $f(z, \theta; \Sigma^{(0)}, \mathcal{V})$ is identical to the difference $f^{(1)}$ between the known and bifurcating drop shapes. In short, the perturbation which signals neutral stability is a perturbation to a bifurcating shape family.

This equivalence makes it possible to examine shape stability and branching of shape families simultaneously. However, the nonlinearity of the Young–Laplace equation (2.13) and the complexity of (3.8) and (3.16) require computer-aided analysis. An essentially numerical algorithm that solves the eigenproblem is given in §5. Its working is clarified by examining the special case for which the analysis proceeds in closed form.

4. SPECIAL CASE: CYLINDRICAL DROP

When the dimensionless volume of the captive drop is $\mathcal{V} = 2\pi B$, the perfectly cylindrical form

$$f^{(0)}(z, \theta) = 1, \quad K^{(0)} = \frac{1}{2} - 2\Sigma, \quad (4.1)$$

is an equilibrium configuration at all rotation speeds, and hence for all values of Σ (thus this one form is an entire shape family). If the spacing between the end faces is not too great, the cylindrical shape is stable at low angular velocities but as Σ increases that shape becomes neutrally stable and another shape family branches off. Moreover, as Σ increases still further there are additional points of neutral stability and bifurcation, as we establish in this section. Incidentally, Pimbley (1976) analysed the multiple equilibrium shapes of a planar interface accelerated towards a less dense fluid – the Rayleigh–Taylor problem – in a similar way.

Substituting (4.1) in (3.16) leads to a greatly simplified set of perturbation problems,

$$\mathcal{L} \left\{ \begin{array}{l} \left[\begin{array}{l} f^{(1)} \\ K^{(1)} \end{array} \right] \equiv \left[\begin{array}{l} [(\nabla^2 + 1 + 8\Sigma^{(0)}) \quad -2] \\ \int_0^\pi \int_{-B}^B [\quad] dz d\theta \quad 0 \end{array} \right] \left[\begin{array}{l} f^{(1)} \\ K^{(1)} \end{array} \right] = \left[\begin{array}{l} 0 \\ 0 \end{array} \right], \\ f^{(1)}(-B, \theta) = f^{(1)}(B, \theta) = 0, \quad 0 \leq \theta \leq \pi, \\ f_\theta^{(1)}(z, 0) = f_\theta^{(1)}(z, \pi) = 0, \quad -B \leq z \leq B, \end{array} \right. \quad (4.2)$$

$$\mathcal{L} \left\{ \begin{array}{l} \left[\begin{array}{l} f^{(2)} \\ K^{(2)} \end{array} \right] = \left[\begin{array}{l} [2(1 - 4\Sigma^{(0)})f^{(1)2} + |\nabla f^{(1)}|^2 - 16\Sigma^{(1)}f^{(1)} - 2f_{\theta\theta}^{(1)}] \\ - \int_0^\pi \int_{-B}^B f^{(1)2}(z, \theta) dz d\theta \end{array} \right], \\ f^{(2)}(-B, \theta) = f^{(2)}(B, \theta), \quad 0 \leq \theta \leq \pi, \\ f_\theta^{(2)}(z, 0) = f_\theta^{(2)}(z, \pi), \quad -B \leq z \leq B, \end{array} \right. \quad (4.3)$$

and similarly for the higher-order problems. Here $\nabla^2 f \equiv f_{zz} + f_{\theta\theta}$ and $|\nabla f|^2 \equiv f_z^2 + f_\theta^2$. The solution of (4.2) gives the points of bifurcation $\Sigma_n^{(0)}$ and first-order approximations $f_n^{(1)}(z, \theta)$ to the shape difference between the cylindrical form and the less symmetric drop form bifurcating from it. The condition for a solution of the inhomogeneous problem (4.3),

$$\langle f_n^{(1)}, \{2(1 - 4\Sigma_n^{(0)})f_n^{(1)2} + |\nabla f_n^{(1)}|^2 - 16\Sigma_n^{(1)}f_n^{(1)} + 2f_n^{(1)}f_{n\theta\theta}^{(1)}\} \rangle - 2K_n^{(1)}\langle f_n^{(1)}, f_n^{(1)} \rangle = 0, \quad (4.4)$$

yields the first-order term $\Sigma_n^{(1)}$ in the expansion (3.14):

$$\Sigma_n^{(1)} = \frac{\langle f_n^{(1)}, \{2(1 - 4\Sigma_n^{(0)})f_n^{(1)2} + |\nabla f_n^{(1)}|^2 + 2f_n^{(1)}f_{n\theta\theta}^{(1)} - 2K_n^{(1)}f_n^{(1)2}\} \rangle}{16 \langle f_n^{(1)}, f_n^{(1)} \rangle}. \quad (4.5)$$

Since $\Sigma(\epsilon) \approx \Sigma^{(0)} + \epsilon\Sigma^{(1)}$, (4.5) indicates the direction of the branching shape family at the point of neutral stability on the energy surface (see figure 1).

There are two classes of non-cylindrical drop shapes to consider, and it is convenient to do so separately. The first comprises the axisymmetric forms; the second comprises the forms lacking even axial symmetry.

(a) *Bifurcations to axisymmetric drop shapes*

When radius f is independent of azimuthal angle θ the solution to (4.2) is simply

$$\left. \begin{aligned} f^{(1)}(z) &= A_1 \sin \gamma z + A_2 [\cos \gamma z - \sin(\gamma z)/B], \\ K^{(1)} &= (A_2 \gamma / 2B) \sin \gamma B, \quad \gamma \equiv (1 + 8\Sigma^{(0)})^{\frac{1}{2}}. \end{aligned} \right\} \quad (4.6)$$

The ratio of A_1 to A_2 is dictated by the boundary conditions in (3.16), which also yield for γ the characteristic equation

$$\sin(\gamma B) [\cos \gamma B - \sin(\gamma B)/\gamma B] = 0. \quad (4.7)$$

This plainly has two types of roots. These can be distinguished on the basis of symmetry about the midplane $z = 0$ between the end faces, and give rise to two types of eigenvalues and eigenfunctions:

Reflectively antisymmetric (r.a.), $n = 1, 2, \dots$

$$\left. \begin{aligned} \sin \gamma_{na} B &= 0, \quad \Sigma_{na}^{(0)} = n^2 \pi^2 / 8B^2 - \frac{1}{8}, \\ f_{na}^{(1)}(z) &= A_{1,n} \sin n\pi z / B, \\ K_{na}^{(1)} &= 0, \quad A_{1,n} = (\pi B)^{-\frac{1}{2}}. \end{aligned} \right\} \quad (4.8)$$

Reflectively symmetric (r.s.), $n = 1, 2, \dots$

$$\left. \begin{aligned} \alpha_{ns} \cot \alpha_{ns} &= 1, \quad \alpha_{ns} \equiv \gamma_{ns} B, \quad \Sigma_{ns}^{(0)} = \alpha_{na}^2 / 8B^2 - \frac{1}{8}, \\ f_{ns}^{(1)}(z) &= A_{2,n} [\cos \gamma_{ns} z - \cos \alpha_{ns}], \\ K_{ns}^{(1)} &= A_{2,n} \alpha_{na} \sin \alpha_n / 2B^2, \quad A_{2,n} = (\pi B \sin^2 \alpha_{na})^{-\frac{1}{2}} \end{aligned} \right\} \quad (4.9)$$

The roots of $\alpha \cot \alpha = 1$ are tabulated (Carslaw & Jaeger 1959). The constants $A_{1,n}$ and $A_{2,n}$ have been determined from the definition of the amplitude parameter ϵ , (3.15), evaluated at first order, namely

$$1 = \pi \int_{-B}^B [f_n^{(1)}(z)]^2 dz. \quad (4.10)$$

The two types of eigenvalues are interlaced, the lowest eigenvalue belonging to an r.s. eigenfunction: see table 1. The successive eigenvalues correspond to points of neutral stability at which new shape families bifurcate from the cylindrical form, each new family having a more wavy profile than the one before. The r.s. and r.a. forms are distinguished by the directions in which the respective families branch from the cylindrical form. These directions are given by $\Sigma_n^{(1)}$, which from (4.5), (4.8) and (4.9) has the values

$$\text{type r.a.:} \quad \Sigma_{ns}^{(1)} = 0, \quad (4.11)$$

$$\text{type r.s.:} \quad \Sigma_{na}^{(1)} = \alpha_n / (\pi B)^{\frac{1}{2}} (B^2 - 5). \quad (4.12)$$

TABLE 1. ROTATIONAL BOND NUMBERS AT WHICH FAMILIES OF REFLECTIVELY SYMMETRIC (R.S.) AND REFLECTIVELY ANTISYMMETRIC (R.A.) SHAPE FAMILIES BIFURGATE FROM THE ROTATING LIQUID CYLINDER

mode number, n	bifurcation point for r.a.-shape family, equation (4.8)	bifurcation point for r.s.-shape family, equation (4.9)
1	$1.237/B^2 - \frac{1}{8}$	$2.5238/B^2 - \frac{1}{8}$
2	$4.9348/B^2 - \frac{1}{8}$	$7.4600/B^2 - \frac{1}{8}$
3	$11.1033/B^2 - \frac{1}{8}$	$14.8622/B^2 - \frac{1}{8}$
4	$19.7392/B^2 - \frac{1}{8}$	$24.7320/B^2 - \frac{1}{8}$

Thus in the $\Sigma\epsilon$ -plane (cf. figure 1) the r.s. family cuts the cylindrical family at an angle that depends on the (dimensionless) length of the captive drop, $2B$. If $B \leq \alpha_n/\sqrt{5}$, $\Sigma_{na}^{(1)}$ is negative and the r.s. family branches off as shown in figure 3. On the other hand, the r.a. family cuts the cylindrical family at right angles and to tell whether the r.a. family extends to higher or lower angular velocities requires finding the curvature of the branch at the intersection, i.e. $\Sigma_{ns}^{(2)}$ in the expansion $\Sigma_{ns} \approx \Sigma_{ns}^{(0)} + \epsilon \Sigma_{ns}^{(1)} + \epsilon^2 \Sigma_{ns}^{(2)}$. This quantity is given by the condition for a solution of the third-order problem, which is inhomogeneous, of course:

$$\langle f_{na}^{(1)}, [6(1 - 4\Sigma_{na}^{(0)})f_{na}^{(1)}f_{na}^{(2)} - 24\Sigma_{na}^{(2)}f_{na}^{(1)} - 4f_{na}^{(1)3} - f_{na}^{(1)}f_{na,z}^{(2)*} + 9f_{na,zz}^{(1)}f_{na,z}^{(1)*}] \rangle = 0. \quad (4.13)$$

This can be rearranged to give

$$\Sigma_{na}^{(2)} = \frac{\langle f_{na}^{(1)} [6(1 - 4\Sigma_{na}^{(0)})f_{na}^{(1)}f_{na}^{(2)} - 4f_{na}^{(1)3} + f_{na}^{(1)}f_{na,z}^{(2)*} + 9f_{na,zz}^{(1)}f_{na,z}^{(1)*}] \rangle}{24\langle f_{na}^{(1)}, f_{na}^{(1)} \rangle}, \quad (4.14)$$

To proceed, it is necessary to work out the r.a. solution to the second-order problem (4.3):

$$\left. \begin{aligned} f_{na}^{(2)}(z) &= B_{1n} \cos(\gamma_{na} z) + B_{2n} \sin(\gamma_{na} z) \\ &\quad + (A_{2n}^2/\gamma_{na}^2) [3 \cos(\gamma_{na} z) - \cos^4(\gamma_{na} z) - \sin^4(\gamma_{na} z)] - (2K_{na}^{(2)} + \gamma_{na}^2 A_{2n}^2)/\gamma_{na}^2 \\ K_{ns}^{(2)} &= \frac{1}{4}(A_{2,n})^2 (3 - \gamma_n^2), \quad \gamma_n \equiv (1 + 8\Sigma_n^{(0)})^{\frac{1}{2}}, \\ B_{1,n} &= (-1)^n [3B/n^2\pi^2 + (A_{2,n})^2 (1 - 2/\gamma_n^2)], \\ B_{2,n} &= 0, \quad n = 1, 2, \dots \end{aligned} \right\} \quad (4.15)$$

Substituting these results in (4.14) yields

$$\Sigma_{ns}^{(2)} = BA_{1n}^2 [-9 - 27\gamma_n^2 + 7\gamma_n^4 - 9\gamma_n^6]/96\gamma_n, \quad n = 1, 2, \dots \quad (4.16)$$

Because this is always negative, the r.s. branches are all curved toward lower Σ and thus the new shape family evolves toward lower angular velocities, as shown in figure 3.

Apart from bifurcation, the stability of cylindrical captive drops with respect to axisymmetric disturbances is governed by an eigenproblem that is a specialization of (3.8):

$$\mathcal{L} \begin{bmatrix} \eta(z, \theta) \\ \beta \end{bmatrix} = \lambda \begin{bmatrix} \eta(z, \theta) \\ 0 \end{bmatrix}, \quad (4.17)$$

$$\eta(-B, \theta) = \eta(B, \theta) = 0, \quad 0 \leq \theta \leq \pi,$$

$$\eta_\theta(z, 0) = \eta_\theta(z, \pi) = 0, \quad -B \leq z \leq B.$$

This was solved by Hardy & Coriell (1974). The eigenfunction and shape perturbation corresponding to the lowest eigenvalue, λ_1 , are called the most dangerous. For the cylindrical shape the most dangerous perturbation is the r.s. type with $n = 1$, for which

$$\lambda_1 = 1 + 8\Sigma - \pi^2/B^2. \quad (4.18)$$

Thus at $\Sigma = \Sigma_{1s}^{(0)} = \pi^2/8B^2 - \frac{1}{8}$ the cylindrical shape loses stability with respect to the r.s.-type of perturbation with $n = 1$, and remains unstable at all higher values of Σ , i.e. at higher angular velocities.

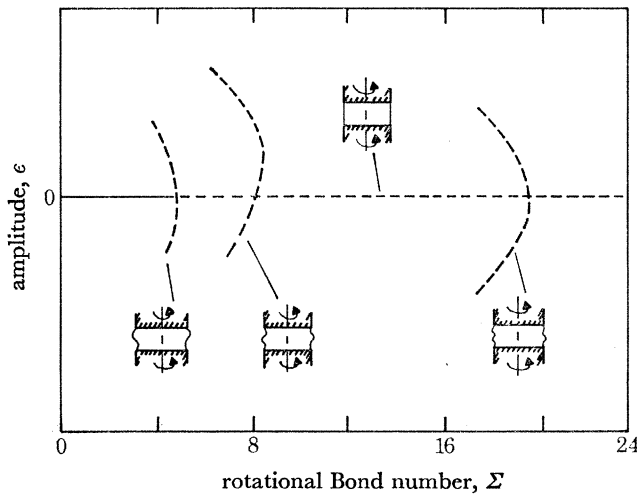


FIGURE 3. Axisymmetric shape families predicted by bifurcation analysis. The drop volume $\mathcal{V} = 2\pi B$ is that of a liquid cylinder between the circular end faces; the drop length is $2B = 1$.

Stability in the shape families that branch from the cylindrical form is another matter. Conventional analysis is limited to the neighbourhood of each bifurcation in which the expansions (3.14) are valid. To assess their range of validity in practice takes comparison with the results of the computer-aided analysis described below, which is not so limited in its applicability.

(b) *Bifurcations to nonaxisymmetric drop shapes*

When the radius f depends on azimuthal angle θ it is necessarily periodic:

$$f(z, 0) = f(z, 2\pi), \quad f_\theta(z, 0) = f_\theta(z, 2\pi), \quad -B \leq z \leq B. \quad (4.19)$$

With these boundary conditions the solutions to (4.2) are again divided into two types according to their midplane symmetry:

Reflectively antisymmetric (r.a.), $n = 1, 3, 5, \dots, k = 1, 2, \dots$

$$\left. \begin{aligned} \Sigma_{nk}^{(0)} &= n^2\pi^2/32B^2 + \frac{1}{8}k^2 - \frac{1}{8}, \\ f_{nk}^{(1)} &= \cos(n\pi z/2B) (C_{1, nk} \cos k\theta + D_{1, nk} \sin k\theta). \end{aligned} \right\} \quad (4.20)$$

Reflectively Symmetric (r.s.), $n = 2, 4, 6, \dots, k = 1, 2, \dots$

$$\left. \begin{aligned} \Sigma_{nk}^{(0)} &= n^2\pi^2/32B^2 + \frac{1}{8}k^2 - \frac{1}{8}, \\ f_{nk}^{(1)}(z, \theta) &= \sin(n\pi z/2B) (C_{2, nk} \cos k\theta + D_{2, nk} \sin k\theta). \end{aligned} \right\} \quad (4.21)$$

Within each type the solutions are paired, the members of a pair corresponding to one and the same shape in two orientations that are related by rotation through 90° about the axis of drop rotation. The two in fact can be combined linearly to give the shape any orientation about the axis. It is convenient to remove this arbitrariness by taking the plane $\theta = 0, \pi$ through the axis to be a reflexion plane of the nonaxisymmetric shape. This requirement forces $D_{1, nk}$ and $D_{2, nk}$ to be zero.

The rotational Bond numbers $\Sigma_{nk}^{(0)}$ are the bifurcation points from the cylindrical family to families of non-axisymmetric drop shapes that nearby have shape perturbations $f_{nka}^{(1)}$ and $f_{nks}^{(1)}$ from the cylinder. The first of these families bifurcates at $\Sigma = \Sigma_{11}^{(0)} = \pi^2/32B^2$ and its nearby members are given by (ϵ small)

$$f(z, \theta) = 1 + \epsilon \cos(\pi z/2B) \cos \theta. \quad (4.22)$$

This is called the C-mode family because all members are bulged out from the axis of rotation at $\theta = 0$ and are dished in toward the axis at $\theta = \pi$.

The stability of the cylindrical drop shape to nonaxisymmetric shape perturbations was studied by Fowle *et al.* (1976), who found that the eigenproblem (3.14) has eigenfunctions and eigenvalues

$$\eta_{nk}(z, \theta) = \begin{cases} \cos(n\pi z/2B) \cos k\theta, & n = 1, 3, 5, \dots \\ \sin(n\pi z/2B) \cos k\theta, & n = 2, 4, 6, \dots \end{cases}, \quad k = 1, 2, \dots, \quad (4.23)$$

$$\eta_{nk} = 1 + 8\Sigma + k^2 - n^2\pi^2/4B^2. \quad (4.24)$$

The cylindrical drop first becomes neutrally stable with respect to a C-mode perturbation at $\Sigma = \Sigma_{11}^{(0)} = \pi^2/32B^2$. Beyond $\Sigma_{11}^{(0)}$ the cylinder is an unstable equilibrium form; C-mode disturbances lower the energy of the drop.

However, *long* cylindrical drops do not first become unstable to C-mode perturbations; they succumb sooner to axisymmetric wavy disturbances, as Fowle *et al.* (1976) showed. Comparison of equations (4.18) and (4.24) shows that the drop length of cross-over is $B = \sqrt[3]{\frac{3}{2}}\pi$: cylindrical drops shorter than this first lose stability to C-mode perturbations; longer ones, to r.s. type axisymmetric disturbances with $n = 1$. In the limit of zero angular velocity this result is equivalent to Rayleigh's (1879) result for the infinitely long cylinder, in that the largest cylinder that is stable has (dimensionless) length 2π .

5. COMPUTER-AIDED ANALYSIS

We have demonstrated that three-dimensional, equilibrium meniscus shapes are well-analysed by means of expansion in subdomain functions according to the finite element method (Orr *et al.* 1975; Brown *et al.* 1980; Brown 1979). Here we go on and show how to adapt the finite element method to the determination of families of shapes, their stability and their branching; in short, the family tree of captive rotating drops.

(a) Drop shape

A finite element representation of the radial distance to the drop surface begins with division of the domain of the governing equations into a convenient set of elements. For present purposes these are segments of the interval $-B \leq z \leq B$ for axisymmetric shapes, and quadrilateral elements within $-B \leq z \leq B$, $0 \leq \theta \leq \pi$ for fully three-dimensional shapes. The next step is to

choose basis functions $\Phi^i(z, \theta)$ for the representation, which is generally no more than an approximation because an infinite number of functions is usually required for a complete basis. Then

$$f(z, \theta) = \sum_{i=1}^{N_D} \alpha_i \Phi^i(z, \theta) + \sum_{i=1}^{N_B} \omega_i \Phi^i(z, \theta), \quad (5.1)$$

where the coefficients α_i and ω_i are to be determined. N_B is the number of basis functions that are non-zero along the bounding contact lines and N_D is the total number of other basis functions. The functions chosen here are either quadratic or cubic polynomials, each being non-zero except in the elements surrounding a particular vertex, or node, between elements. This set of elements constitutes a subdomain.

For axisymmetric shapes we employ Hermite cubic polynomials (Strang & Fix 1973, p. 55), two of which are defined at each vertex $z = z_i$:

$$\Phi_j^i = a_j^i + b_j^i z + c_j^i z^2 + d_j^i z^3. \quad (5.2)$$

The constants are so chosen that $\Phi_1^i(z)$ is unity and has zero slope at z_i , it and its slope vanishing at other vertices; whereas $\Phi_2^i(z)$ is zero at z_i but has unit slope there and together with its slope vanishes at other vertices:

$$\left. \begin{aligned} \Phi_1^{(i)}(z_j) &= \delta_{ij}, & d\Phi_1^{(i)}(z_j)/dz &= 0, \\ \Phi_2^{(i)}(z_j) &= 0, & d\Phi_2^{(i)}(z_j)/dz &= \delta_{ij}, \end{aligned} \right\} \quad (5.3)$$

(δ_{ij} is the Dirac delta). For three-dimensional menisci our choice here is the so-called reduced quadratic basis (Strang & Fix 1973, p. 83). The vertices and points midway along the side of each quadrilateral are designated as nodes, associated with each of which is a quadratic polynomial

$$\Phi_i(z, \theta) = a_{1i} + a_{2i} z + a_{3i} \theta + a_{4i} \theta z + a_{5i} z^2 + a_{6i} \theta^2 + a_{7i} z^2 \theta + a_{8i} \theta^2 z. \quad (5.4)$$

The eight constants are so chosen that $\Phi_i(z, \theta)$ is unity at the i th node and vanishes at all other nodes. Thus, within a given element the approximation basis consists of functions associated with nodes on its boundary, each of these functions being non-zero only on a subdomain made up of elements that share the node. In this sense the finite element method makes use of overlapping subdomains.

The coefficients in (5.1) are now the values of the radial function at the nodes. The contact line boundary condition is incorporated into the finite element scheme by specifying the coefficients along the boundary, i.e. $\omega_i = 1$, $i = 1, 2, \dots, N_B$.

With a finite set of basis functions the mathematically infinite-dimensional extremum problem (2.12) for equilibrium drop shape reduces to a finite-dimensional one, the number of dimensions being $N_D + 1$. The conditions for an equilibrium shape are simply that the partial derivatives of the augmented effective kinetic potential (2.11) with respect to the coefficients α_i be zero:

$$\begin{aligned} R_i(\alpha, K) &\equiv \partial \mathcal{K} / \partial \alpha_i, \quad i = 1, \dots, N_D, \\ &= \int_0^\pi \int_{-B}^B \left[\frac{f \Phi^i + f f_z^2 \Phi^i + f^2 f_z \Phi_z^i + f_\theta \Phi_\theta^i}{(f^2 + f^2 f_z^2 + f_\theta^2)^{\frac{1}{2}}} - 4 \Sigma f^3 \Phi^i - 2 K f \Phi^i \right] dz d\theta = 0. \end{aligned} \quad (5.5)$$

There is also an equation from the condition of fixed volume (2.7):

$$R_{N_D+1}(\alpha, K) = \mathcal{V} - \frac{1}{2} \int_0^\pi \int_{-B}^B f^2 dz d\theta = 0. \quad (5.6)$$

Substituting the finite element representation (5.1) for $f(z, \theta)$ converts (5.5) and (5.6) into a set of nonlinear, algebraic equations for the unknown coefficients α_i and unknown reference pressure K —in all, $N_D + 1$ unknowns. Once these are found, (5.1) gives the corresponding N_D -dimensional finite element approximation to the drop shape. The accuracy of this solution can be tested by going to a higher-dimensional approximation constructed with a larger number of smaller elements or higher-order polynomial basis functions on the same elements.

The method of choice for solving the nonlinear equation set (5.5)–(5.6) is Newton's iteration. Starting from an initial estimate $(\alpha_1^{(0)}, \alpha_2^{(0)}, \dots, \alpha_{N_D}^{(0)}, K^{(0)})$ we determine successive iterates by

$$\begin{bmatrix} \alpha_1^{(k+1)} \\ \vdots \\ \alpha_{N_D}^{(k+1)} \\ \hline K^{(k+1)} \end{bmatrix} = \begin{bmatrix} \alpha_1^{(k)} \\ \vdots \\ \alpha_{N_D}^{(k)} \\ \hline K^{(k)} \end{bmatrix} - \begin{bmatrix} \frac{\partial^2 \mathcal{H}}{\partial \alpha_1^2} & \cdots & \frac{\partial^2 \mathcal{H}}{\partial \alpha_1 \partial \alpha_{N_D}} & \left| \frac{\partial^2 R_{N_D+1}}{\partial \alpha_1} \right. \\ \vdots & & \vdots & \vdots \\ \frac{\partial^2 \mathcal{H}}{\partial \alpha_{N_D} \partial \alpha_1} & \cdots & \frac{\partial^2 \mathcal{H}}{\partial \alpha_{N_D}^2} & \left| \frac{\partial^2 R_{N_D+1}}{\partial \alpha_{N_D}} \right. \\ \hline \frac{\partial^2 \mathcal{H}}{\partial K \partial \alpha_1} & \cdots & \frac{\partial^2 \mathcal{H}}{\partial K \partial \alpha_{N_D}} & \left| 0 \right. \end{bmatrix}^{-1} \begin{bmatrix} R_1^{(k)} \\ \vdots \\ R_{N_D}^{(k)} \\ \hline R_{N_D+1}^{(k)} \end{bmatrix}. \quad (5.7)$$

This represents a large system of linear equations at each iteration, but the Jacobian matrix here is not only symmetric, but also sparse, the non-zero elements clustering about the main diagonal (because only neighbouring subdomains overlap). The matrix is easily stored in computer memory by profile methods (Bathe & Wilson 1976) and the set of linearized equations is readily solved by direct factorization of this Jacobian matrix (Bathe & Wilson 1976). The Newton iteration is continued until the largest change in the correction vector, i.e. the differences $\alpha_i^{(k+1)} - \alpha_i^{(k)}$ and $K^{(k+1)} - K^{(k)}$, is less than 10^{-8} .

Because a captive drop may have more than one equilibrium shape, the nonlinear equation set (5.5)–(5.6) may have multiple solutions. The one found by a Newton iteration, if the iteration converges at all, depends crucially on the initial estimate $(\alpha^{(0)}, K^{(0)})$ and the shape of the energy surface between that estimate and the solution(s). As indicated by the dashed lines in figure 1, for each value of the parameter Σ there are domains of attraction about each equilibrium shape solution, such that Newton iterations which begin with a shape within a given domain converge to the solution in that domain. The limits of such domains no doubt relate to the lines of inflexion on the energy surface (see figure 1). In tracing out shape families as Σ is changed, we use the last solution to start the iteration for the next. The larger the step in Σ , the slower the rate of convergence of the Newton iteration, until it fails to converge (underrelaxation may restore convergence provided the step in Σ is not too large). Plainly there is an optimal strategy for tracing out a shape family. There can also be difficulty near a point of bifurcation, as discussed below.

(b) Stability and bifurcation

The stability of each equilibrium shape is calculated from the constrained eigenproblem (3.4)–(3.5), which simultaneously reveals whether a new shape family branches from that shape. The shape perturbations that are considered are all of those that can be represented in the same finite element basis (5.1) as the solution, and which likewise leave the meniscus pinned to the edges of the solid faces that hold the drop captive:

$$\eta(z, \theta) = \sum_{i=1}^{N_D} x_i \Phi^i(z, \theta). \quad (5.8)$$

The truncated expansions (5.1) and (5.8) reduce the Rayleigh quotient (3.4) to its analogue for the N_D -dimensional function space:

$$\lambda_i = \min_{\mathbf{x} \in \mathbb{R}^{N_D}} \frac{\mathbf{x}^T \mathbf{J} \mathbf{x}}{\mathbf{x}^T \mathbf{M} \mathbf{x}}, \quad (5.9)$$

over all linear combinations of N_D -dimensional vectors that satisfy the requirements

$$\mathbf{c}^T \mathbf{x} = 0, \quad \mathbf{x}_j^T \mathbf{x}_i = 0, \quad j < i, \quad (5.10)$$

where \mathbf{J} is the Hessian, or energy sensitivity, matrix ($J_{ij} \equiv \partial^2 \mathcal{E} / \partial \alpha_i \partial \alpha_j$), \mathbf{M} is the basis function overlap matrix ($M_{ij} \equiv \langle \phi^i, \phi^j \rangle$), and \mathbf{c} is the shape function projection vector ($c_i \equiv \langle f, \phi^i \rangle$). Both \mathbf{J} and \mathbf{M} are symmetric. Moreover, \mathbf{M} , sometimes called a ‘mass matrix’ in finite element literature, is positive definite.

The minimization problem (5.9) is readily converted to a constrained, generalized eigenproblem:

$$\mathbf{J} \mathbf{x}_i = \lambda_i \mathbf{M} \mathbf{x}_i, \quad \mathbf{c}^T \mathbf{x}_i = 0, \quad i = 1, 2, \dots, N_D. \quad (5.11)$$

The eigenvalues are necessarily real. It is convenient to order them from the smallest to the largest. Negative eigenvalues signal instability with respect to shape perturbations described by the corresponding eigenvector \mathbf{x}_i . For (5.8) to be a good approximation to an eigenvector that corresponds to an irregular shape, the dimension of the finite basis, N_D , may have to be quite large (250 or more). Established techniques of matrix transformation for solving (5.11) (see, for example, Moler & Stewart 1973) destroy matrix sparsity and therefore require storage of both \mathbf{J} and \mathbf{M} . Few computers, including the CDC Cyber 74 available to us, have a large enough central memory, and so iterative methods must be used.

For (5.11) we prefer the block-Lanczos method recently developed by Golub & Underwood (1977) and adapted as explained here. For the simple eigenproblem

$$\mathbf{A} \mathbf{z}_i = \mu_i \mathbf{z}_i, \quad i = 1, 2, \dots, N_D, \quad (5.12)$$

where \mathbf{A} is positive definite and symmetric, the method computes the lowest several eigenvalues and their eigenvectors. In each iteration the only operation involving \mathbf{A} is multiplication by a vector, and thus any sparsity of \mathbf{A} is preserved. The rate at which the method converges on an eigenvalue depends on the initial estimate of the eigenvector, on the spacings of the eigenvalues, and on their spread $|\lambda_{N_D} - \lambda_1|$ (Underwood 1975). The spread is large for (5.11), from large positive eigenvalues corresponding to disturbances stabilized by surface tension, to a small positive or even negative value for the most dangerous shape disturbance, i.e. the first to give rise to instability as Σ is varied.

To convert (5.11) to the standard form (5.12) we transform it by means of the relations

$$\hat{\mathbf{J}} \equiv \mathbf{J} + s\mathbf{M} = \mathbf{L}\mathbf{L}^T, \quad s > 0, \quad (5.13)$$

$$1/\mu_i \equiv \lambda_i + s \quad s > 0, \quad (5.14)$$

where s is chosen large enough that $\hat{\mathbf{J}}$ is positive definite, and where \mathbf{L} is the lower triangular matrix resulting from a Cholesky factorization of $\hat{\mathbf{J}}$ (Wilkinson 1965). The result is

$$\left. \begin{aligned} \mathbf{L}^{-1}(-\mathbf{M})\mathbf{L}^{-T} \mathbf{y}_i = \mu_i \mathbf{y}_i, \quad \mathbf{d}^T \mathbf{y}_i = 0, \quad i = 1, 2, \dots, N_D, \\ \mathbf{y}_i \equiv \mathbf{L}^T \mathbf{x}_i, \quad \mathbf{d} \equiv \mathbf{L}^{-1} \mathbf{c}, \quad \mathbf{d}^T \mathbf{d} = 1. \end{aligned} \right\} \quad (5.15)$$

The eigenvalues are bounded:

$$-1/(\lambda_1 + s) \leq \mu_i \leq -1/(\lambda_{N_D} + s). \quad (5.16)$$

The orthogonality constraint $d^T \mathbf{y}_i = 0$ is satisfied by making use of the projection operator onto the subspace of volume-conserving perturbations, as outlined by Golub (1973):

$$\mathbf{P} \equiv \mathbf{I} - \mathbf{d}\mathbf{d}^T, \quad (5.17)$$

where \mathbf{I} is the identity matrix. The problem (5.15) is transformed to

$$\mathbf{A}\mathbf{z}_i = [\mathbf{P}\mathbf{L}^{-1}(-\mathbf{M})\mathbf{L}^{-T}\mathbf{P}]\mathbf{z}_i = \mu_i \mathbf{z}_i, \quad i = 1, 2, \dots, N_D, \quad (5.18)$$

where \mathbf{z}_i is any N_D -dimensional vector. The eigenvectors here and in (5.15) are related by $\mathbf{y}_i = \mathbf{P}\mathbf{z}_i$ and the eigenvalues are identical. The matrix \mathbf{A} is positive definite and symmetric and its eigenvalues and eigenvectors are found by the block-Lanczos method. We require the eigenpair to satisfy the convergence criterion $\|\mathbf{A}\mathbf{z}_i - \mu_i \mathbf{z}_i\|_2 \leq 10^{-6}$ where $\|\cdot\|_2$ is the N_D -dimensional Euclidean norm (Wilkinson 1965, p. 57).

The eigenvectors and eigenvalues of the original form of the stability problem (5.9) are recovered from

$$\mathbf{x}_i = \mathbf{L}^{-T}\mathbf{P}\mathbf{z}_i, \quad \lambda_i = -s + 1/\mu_i. \quad (5.19)$$

If \mathbf{A} in (5.18) were actually formed it would not be sparse. However, this matrix is not stored in the computer's memory. Just the sparse matrices \mathbf{L} and \mathbf{M} are stored, and the product of \mathbf{A} with any vector is constructed by operations involving only solution of triangular systems of equations and matrix-vector multiplications. Profile storage methods (Bathe & Wilson 1976) prove advantageous.

The eigenvectors \mathbf{x}_i are finite element approximations to the normal modes of the drop shape, from which come \mathbf{J} and \mathbf{c} ; the eigenvalues λ_i if positive are related (through inertial quantities) to the natural oscillation frequencies in the respective modes. Stability is of course governed by the sign of the *lowest* eigenvalue $\lambda_1 (= \mu_1^{-1} - s)$ which, if negative, indicates instability. On the other hand, as the parameter \mathcal{Z} is varied, any point at which any eigenvalue λ_j passes through zero is a bifurcation point of the shape family from which come \mathbf{J} and \mathbf{c} . Moreover, the eigenvector \mathbf{x}_j describes the shape difference between the original form and the one bifurcating from it, just as at (3.10), and so a good estimate for a shape nearby on the new branch is

$$f(z, \theta) = f^{(0)}(z, \theta) + \epsilon \sum_{i=1}^{N_D} x_{ji} \Phi^i(z, \theta), \quad (5.20)$$

where x_{ji} are the components of \mathbf{x}_j , and ϵ is the amplitude parameter defined by (3.15). Whether or not this first estimate actually falls in the domain of attraction of a shape on the new branch depends on the original shape $f^{(0)}$ selected – in particular, how close it is to the bifurcation point – and on the amplitude parameter ϵ chosen.

To make the Newton iteration jump over from the original family to the new one near a bifurcation point, we launch iterations from initial estimates given by (5.20) in which ϵ is made successively larger. Invariably we find that when ϵ is small the iteration converges back to $f^{(0)}$ but that when ϵ is somewhat larger the iteration if it converges at all does so to a shape on the new branch. Thus it appears that the domains of attraction near a bifurcation point are qualitatively as figure 1 suggests.

One way of determining whether the new shape family exists at higher or lower values of the parameter \mathcal{Z} is with a higher-order perturbation analysis like that in §4. But such an analysis is not easily incorporated in the algorithm we are describing here, and so we simply test for new shape families by starting Newton iterations with (5.20) as just outlined, but with finite element solutions $f^{(0)}$ at rotational Bond numbers \mathcal{Z} slightly above and slightly below a bifurcation point value.

All the analysis in this section is codified in a computational algorithm for determining equilibrium drop shapes, their stability, and bifurcation of shape families. The algorithm is summarized in figure 4. There are many procedures for tracing out an entire family tree. We usually choose to trace out the new branch from a bifurcation before returning to continue along the original trunk or the older branch. Incidentally, we have not investigated the possibility that additional families of three-dimensional captive drop shapes exist which are not in the tree that is delineated in the next section.

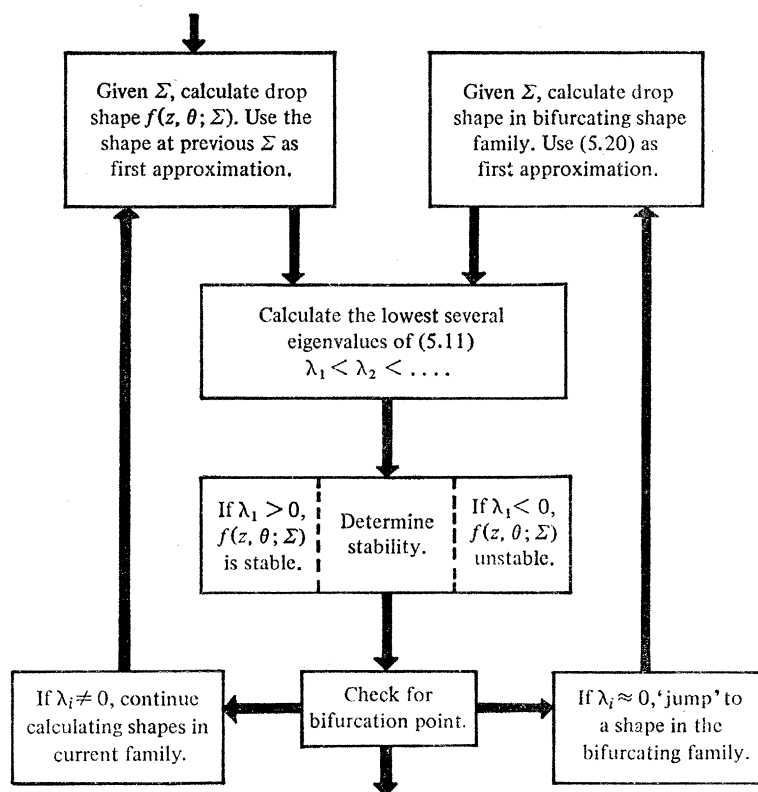


FIGURE 4. Flow chart of finite element algorithm for calculating shape and stability of rotating captive drops.

6. RESULTS

The algorithm was tested by using it to find axisymmetric drop shapes and their stability with respect to axisymmetric disturbances. The basis in both instances was usually 82-dimensional, consisting of Hermite cubic functions on 40 elements spanning the interval $-B \leq z \leq B$. The results for axisymmetric drops having the volume of a cylinder, i.e. $\mathcal{V} = 2\pi B$, are plotted in figure 5, which shows the reflectively symmetric (r.a.) families for $n = 1$ and $n = 2$, the reflectively antisymmetric (r.s.) family for $n = 1$, and the trunk family consisting of the cylindrical drop at all speeds of rotation. The three bifurcation points were estimated by interpolating the eigenvalue results and each is within 0.5% of the corresponding value computed from analytical formulas (4.8) and (4.9). The sample shapes on the branch (r.a., $n = 1$) in figure 6 show profiles that grow more exaggerated as Σ is decreased more and more from the bifurcation value. Ultimately the slope df/dz becomes infinite at some point on the profile and the shape representation $r = f(z)$ fails.

Only one segment in figure 5 consists of shapes stable to axisymmetric disturbances. The results agree with those of §4 in that the cylindrical drop first becomes unstable to an axisymmetric disturbance, namely r.a., $n = 1$, at $\Sigma = \Sigma_{1a}^{(0)} = \pi^2/8B^2 - 1$, the value that Hardy & Coriell (1974) found. The entire family of (r.a., $n = 1$)-shapes is unstable to (r.a., $n = 1$)-disturbances which, though they have roughly the same form as the equilibrium shapes, are *not* perturbations from one to another shape in the family. Except for the cylindrical shape at $\Sigma < \Sigma_{1a}^{(0)}$, all the shape families we investigated with the finite element algorithm – through to $n = 3$ shapes – are unstable to (r.a., $n = 1$) disturbances.

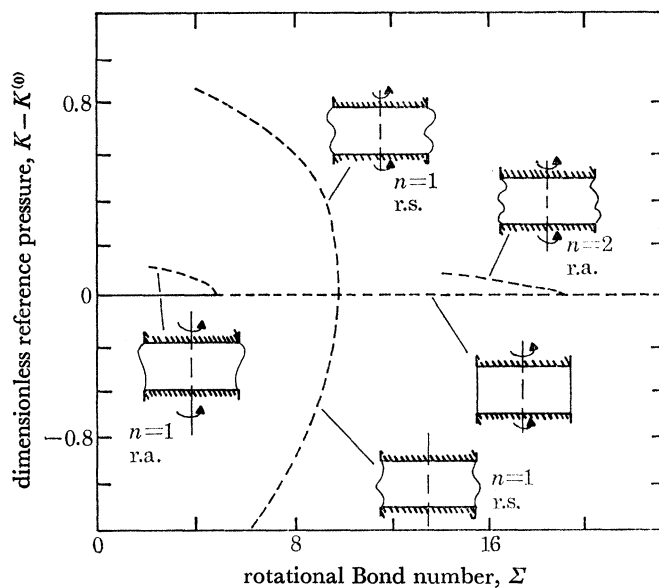


FIGURE 5. Axisymmetric shape families calculated by finite element analysis. The drop volume is $2\pi B$ and the length is $2B = 1$.

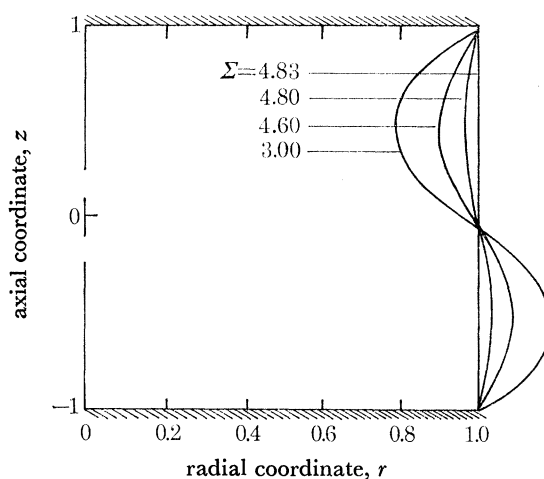
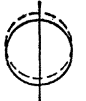
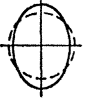




FIGURE 6. Sample profiles (r.a., $n = 1$) of axisymmetric captive drops of volume and length $\mathcal{V} = 2\pi B$ and $2B = 1$, respectively. Σ is the rotational Bond number.

(a) Drops having the volume of a cylinder

Fully three-dimensional shapes and shape perturbations were investigated with 121- and 225-dimensional bases consisting of reduced quadratic finite elements, eight of them in the z -interval and four or eight around the θ -coordinate. The accuracy of the finite element representation of drop shape depends on the departure of the shape from the cylinder and on the dimensionality of

TABLE 2. COMPARISON OF EIGENVALUES CALCULATED BY FINITE ELEMENT ANALYSIS OF THE STABILITY OF A ROTATING CAPTIVE CYLINDER WITH THOSE GIVEN BY (4.24). RESULTS FROM BOTH 4×8 AND 8×8 ELEMENT MESHES ARE SHOWN

cross-section of eigenfunction	λ_{nk}	analytical values equation (4.20)	finite element calculation with 4×8 mesh		finite element calculation with 8×8 mesh	
			value	% relative error	value	% relative error
	λ_{11}	-0.13040	-0.12948	0.071	-0.13003	0.028
	λ_{12}	2.86960	2.90224	1.140	2.87207	0.009
	λ_{13}	7.86960	8.19020	4.074	7.89298	0.297
	λ_{14}	14.86960	18.3236	23.229	14.9226	0.379

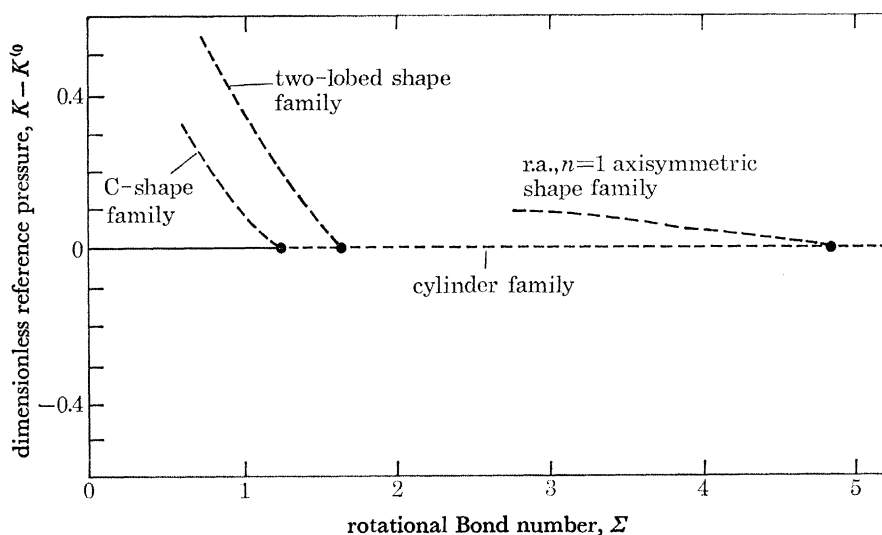


FIGURE 7. Shape families of rotating captive drops of volume and length $\mathcal{V} = 2\pi B$ and $2B = 1$, respectively. The cylinder is an equilibrium shape at all angular velocities.

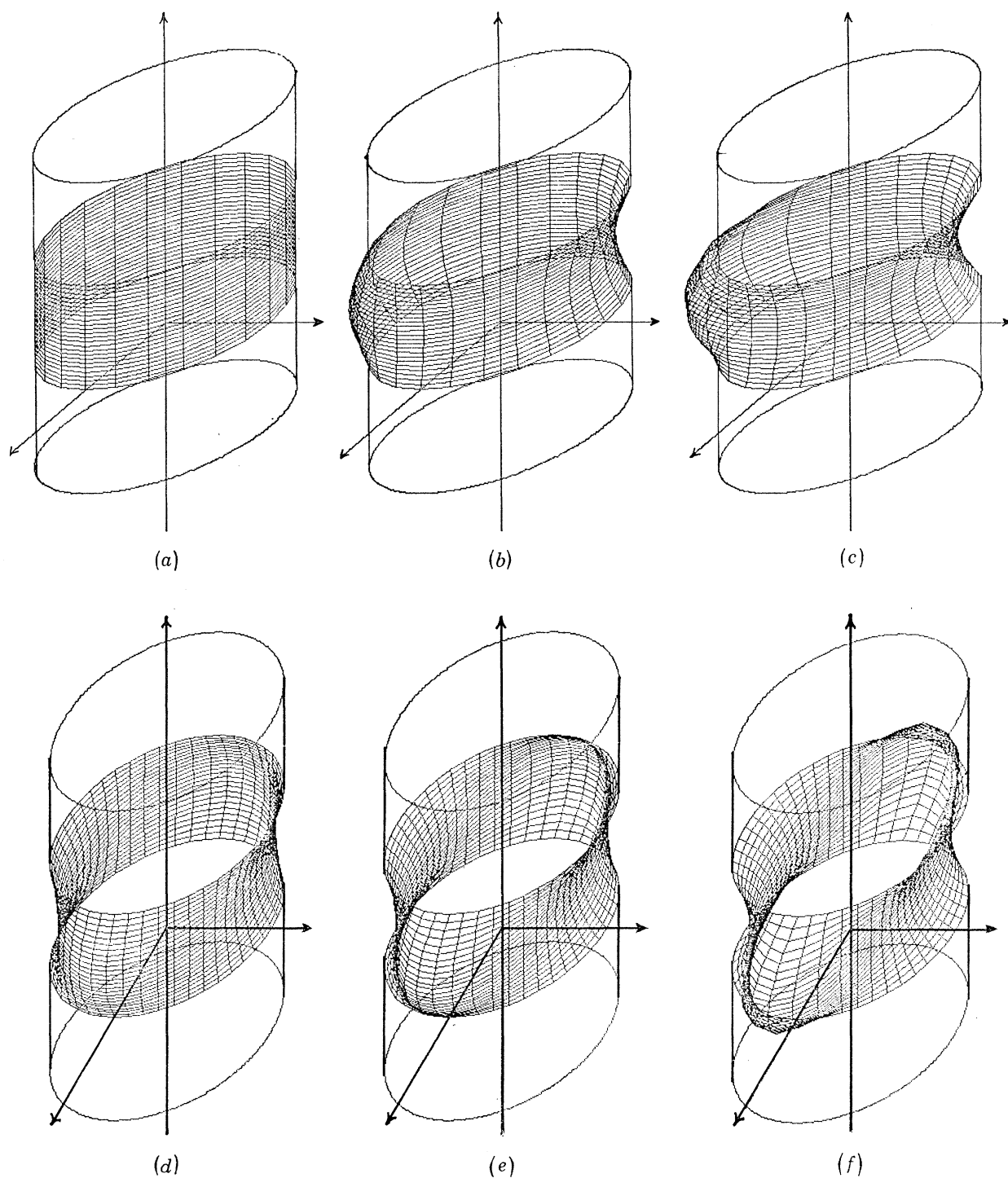


FIGURE 8. Sample C-shaped and two-lobed rotatint captive drops. $\mathcal{V} = 2\pi B$ and $B = 0.5$. (a), $\Sigma = 1.25$, cylinder: stable; (b), $\Sigma = 1$, C-shaped: unstable; (c), $\Sigma = 0.8$, C-shaped: unstable; (d), $\Sigma = 1.5$, two-lobed: unstable; (e), $\Sigma = 1.3$, two-lobed: unstable; (f), $\Sigma = 1$, two-lobed: unstable.

the basis, besides the convergence criterion chosen for the Newton iteration. The accuracy of the finite element solution of the eigenproblem for shape stability also depends on the dimensionality of the basis as well as the convergence criterion adopted from the block-Lanczos method. The accuracies achieved can be inferred from comparisons of the resulting eigenvalues for cylindrical drops with those computed from closed-form formula (4.24). Table 2 is representative. The eigenfunction planforms shown are cross-sections at $z = 0$, as given by (4.23). The 8×4 -element arrangement represents well the most highly symmetric modes but the 8×8 -element arrangement is needed to approximate $k = 3$ and $k = 4$ as well. Thus, among the four lowest eigenvalues, λ_{11} and λ_{12} are calculated quite accurately with the smaller basis but λ_{13} and λ_{14} require the larger basis to obtain accuracy better than 0.4%.

The first and second three-dimensional shape families that branch from the cylindrical family do so at lower values of the rotational Bond number than does the (r.a., $n = 1$)-family, as depicted in figure 7, which is for $B = 0.5$, i.e. a captive drop as long as its radius. As first predicted by Fowle *et al.* (1976) – see §4(b) – the cylindrical drop loses stability with respect to a C-shaped disturbance. At the point of neutral stability we find bifurcation to a family of C-shaped drops, members of which are shown in figure 8. By interpolation the bifurcation is at $\Sigma = \Sigma_{11}^{(0)} \simeq 1.22$; comparison with the value $\Sigma_{11}^{(0)} = 1.23$ computed from analytical formula (4.20) gives another indication of the accuracy of the finite element algorithm as implemented in this study. At a higher rotational Bond number, by interpolation $\Sigma = \Sigma_{12}^{(0)} \simeq 1.62$, which is to be compared with

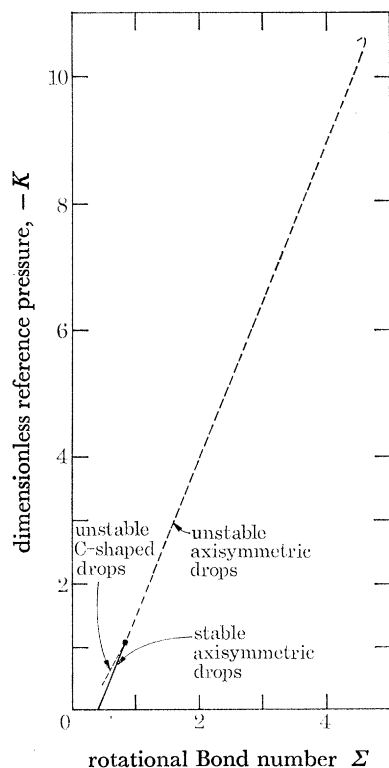


FIGURE 9. Axisymmetric and C-shaped families of fat rotating captive drops. $\mathcal{V} = 2.4\pi B$ and $B = 0.5$. Stable (—) and unstable (---) shapes are shown.

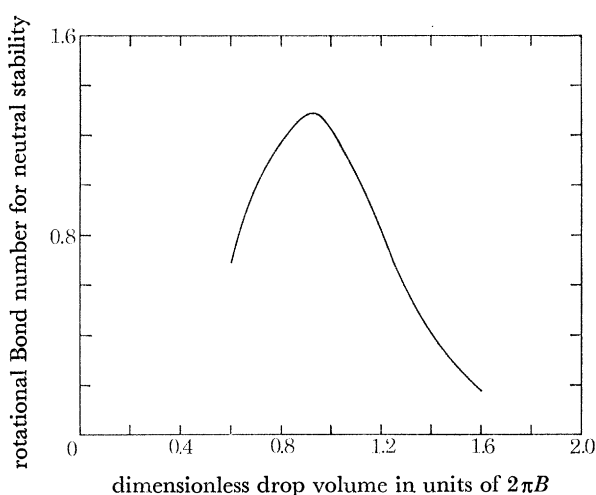


FIGURE 10. Critical value of rotational Bond number for onset of instability of axisymmetric rotating captive drops of length $2B = 1$, as a function of the drop volume. A C-shaped perturbation causes instability in every case.

the value 1.62 from (4.20), there is bifurcation to a family of two-lobe drops, members of which are also shown in figure 8.

The shapes in the C-shaped and two-lobe families are all unstable with respect to C-shaped disturbances where $B = 0.5$ and $\mathcal{V} = 2\pi B$. We found no stable three-dimensional drop shape at rotational speeds greater than $\Sigma_{11}^{(0)}$.

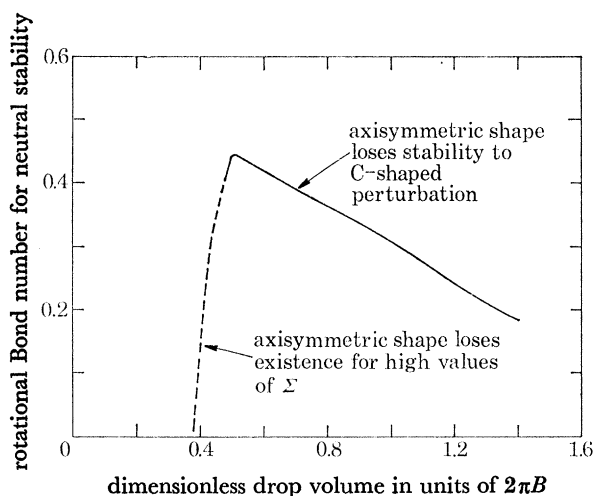


FIGURE 11. Critical value of rotational Bond number for onset of instability of axisymmetric rotating captive drops of length $2B = 2$, as a function of the drop volume.

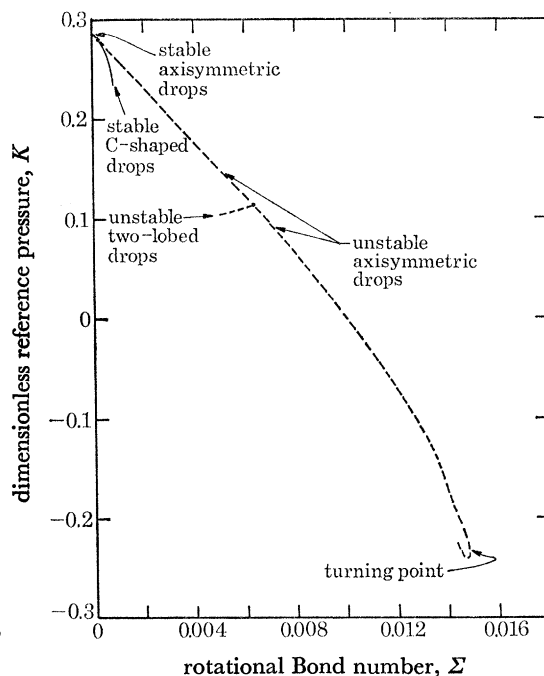


FIGURE 12. Axisymmetric, C-shaped, and two-lobed families of obese rotating captive drops. $\mathcal{V} = 24\pi B$ and $B = 3$. Stable (—) and unstable (---).

(b) *Drops not having the volume of a cylinder*

When drop volume differs from $\mathcal{V} = 2\pi B$ the bifurcation diagram, or family tree, changes in character. Figure 9 show the families of fat captive drops when $\mathcal{V} = 2.4\pi B$ and $B = 0.5$. Axisymmetric shapes do *not* exist for all rotational Bond numbers; they come to an end at $\Sigma \simeq 4.61$. Instability is again first caused by C-mode perturbation and this happens at $\Sigma \simeq 0.819$, beyond which the axisymmetric forms are unstable.

An axisymmetric shape is stable to the highest rate of rotation if it is slightly skinny, at least when $B = 0.5$. The critical value of rotational Bond number Σ for onset of instability is plotted in figure 10 as a function of drop volume when $B = 0.5$, and it can be seen that $\mathcal{V} \simeq 0.95\pi B$ has the greatest stability. Instability, when it does occur, is always with respect to a C-mode when $B = 0.5$.

This is not so when $B = 1$, i.e. for captive drops twice as long as their end radii. The critical value of Σ for onset of instability is plotted in figure 11 as a function of drop volume when $B = 1$. Instability is with respect to a C-mode down to $\mathcal{V} \simeq 0.84\pi B$. Axisymmetric drops with smaller volume not only lose stability, but also fail to exist beyond their critical value of Σ , i.e. these axisymmetric shape families have a turning point there. Just below the critical value there are two axisymmetric shapes at a given rotational Bond number. The shapes in the limb of the

axisymmetric family that ascends to the turning point are stable, whereas those in the limb beyond the turning point are unstable with respect to an axisymmetric (r.a., $n = 1$) perturbation. As the drop volume is decreased the critical value of Σ at which the axisymmetric shapes are lost also decreases, until a limit in volume is reached where no static axisymmetric shape is possible even when the drop is not rotating. The shapes of axisymmetric captive drops that are not rotating are shapes of constant mean curvature and their profiles are sections of either cylinders, spheres,

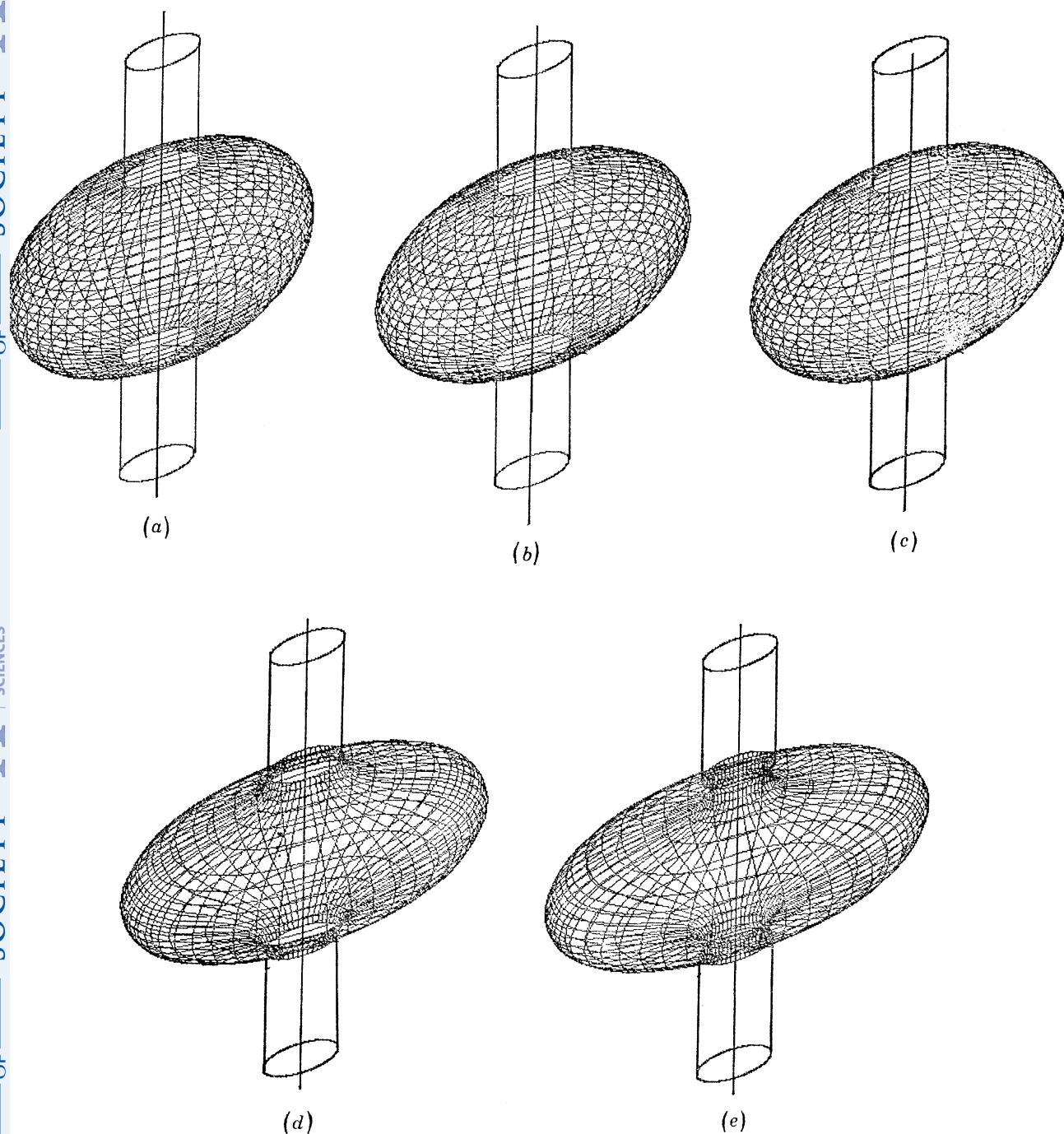


FIGURE 13 (a-e). For descriptions see opposite.

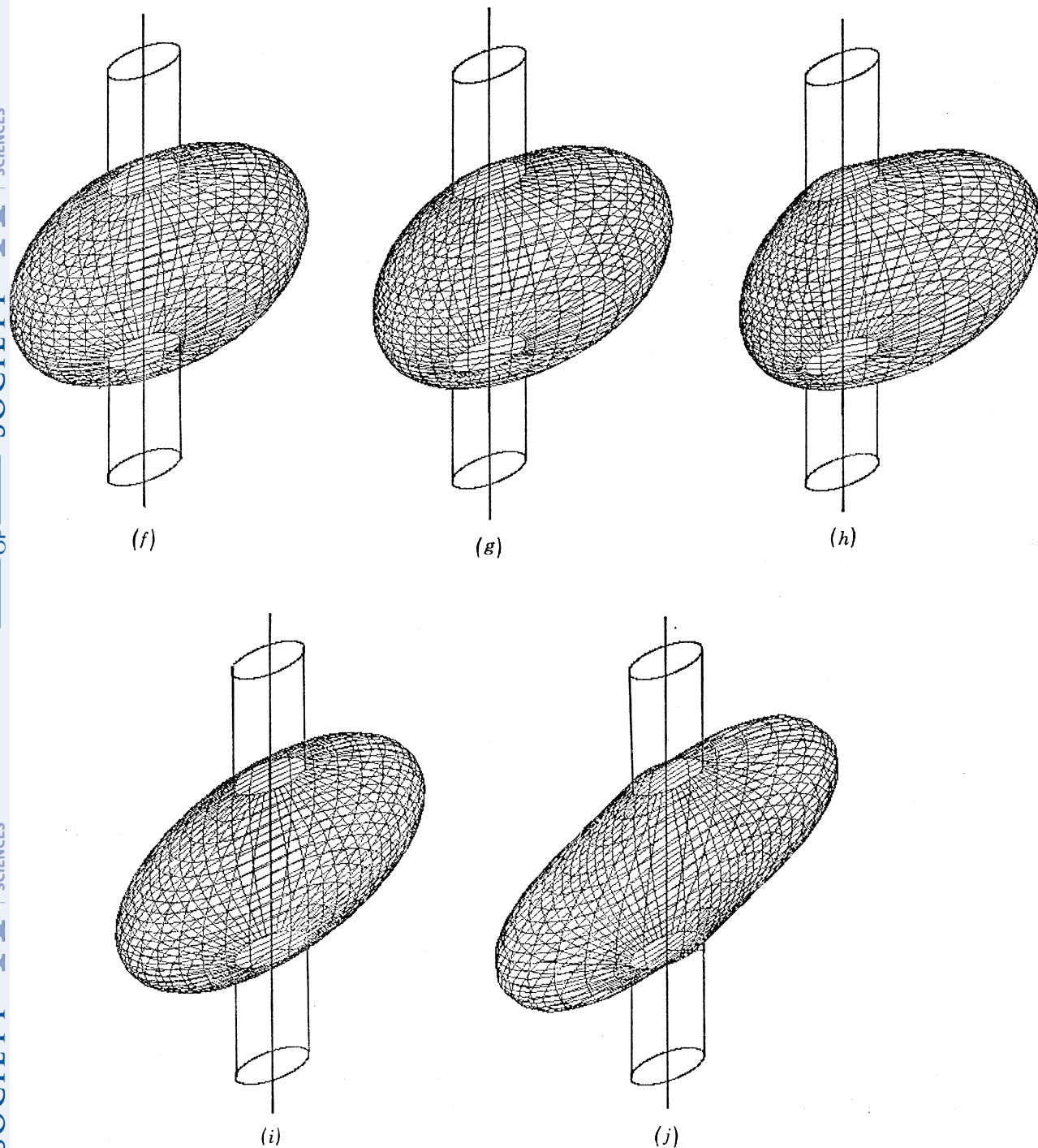


FIGURE 13. Sample shapes from the families of obese rotating captive drops. $\mathcal{V} = 24\pi B$ and $B = 3$. (a), $\Sigma = 0.0002$, axisymmetric: stable; (b), $\Sigma = 0.00034$, axisymmetric: neutrally stable; (c), $\Sigma = 0.0063$, axisymmetric: unstable; (d), $\Sigma = 0.014$, axisymmetric: unstable; (e), $\Sigma = 0.019$, axisymmetric: unstable; (f), $\Sigma = 0.00034$, C-shaped: stable; (g), $\Sigma = 0.004$, C-shaped: stable; (h), $\Sigma = 0.0005$, C-shaped: stable; (i), $\Sigma = 0.006$, two-lobed: unstable; (j), $\Sigma = 0.005$, two-lobed: unstable.

catenoids, nodoids, or unduloids. Gillette & Dyson (1971) studied the stability of static captive drops.

The antithesis of a very skinny captive drop is an obese drop whose cross-sectional radius – measured when the drop is static and axisymmetric – is much larger than the radius of the solid faces. The axisymmetric, C-shaped, and two-lobed shape families for an obese drop with $\mathcal{V} = 24\pi B$ and $B = 3$ are shown in figure 12. The drop is almost spherical at rest, but as its angular velocity is increased the drop expands in the plane perpendicular to the axis of rotation. As shown by the sample shapes in figure 13, at moderate rotation rates the axisymmetric drops become so deformed that only small liquid throats connect the body of the drop to the solid faces. At even higher rotation rates the diameter of these throats is smaller than the diameter of the faces. At $\Sigma = 0.0149$ the axisymmetric shape family turns back to lower values of rotational Bond number. No equilibrium shapes are found at higher rotation rates.

Drops in the axisymmetric shape family become unstable long before the turning point. The obese captive drop with $\Sigma \simeq 0.00031$ is neutrally stable to a C-shaped perturbation. All axisymmetric shapes at higher Σ are unstable to a C-shaped perturbation. At $\Sigma \simeq 0.000623$ a two-lobed perturbation causes neutral stability of the axisymmetric shape; shapes with higher rotational Bond numbers are unstable to both C-shaped and two-lobed perturbations.

The axisymmetric shapes that are neutrally stable to C-shaped and two-lobed perturbations mark bifurcation points to nonaxisymmetric shape families whose members are C-shaped and two-lobed, respectively. Shapes in these families were calculated using the finite element algorithm and sample drop shapes are shown in figure 13.

The C-shaped obese drops bifurcate supercritically from the axisymmetric shapes, i.e., the C-shapes exist for rotational Bond numbers greater than the bifurcation value $\Sigma \simeq 0.00031$. They grow more deformed as the angular velocity increases (figures 13*e–g*) until past $\Sigma \simeq 0.000623$ no equilibrium C-shape can be found. Here the family of C-shaped drops passes through a turning point with respect to rotational Bond number. The shape at the turning point is neutrally stable to a C-shaped perturbation, and past the turning point the C-shapes are unstable to a C-shaped perturbation.

The two-lobed obese drops bifurcate subcritically from the axisymmetric shapes, i.e. the two-lobed shapes exist at Σ lower than the bifurcation value $\Sigma \simeq 0.000623$. As shown by the sample shapes in figures 13(i) and (j), the lobes of the drop elongate as the angular velocity of the drop is decreased. The eigenproblem (5.18) for any two-lobed shape has a negative eigenvalue for a C-shaped eigenfunction; thus all the two-lobed shapes are unstable to a C-shaped perturbation.

7. DISCUSSION

According to the foregoing results, an *axisymmetric* captive drop with fixed contact lines, if it is stable at rest, remains in stable gyrostatic equilibrium at angular velocities of rotation up to a critical value. At this critical angular velocity the axisymmetric drop becomes unstable, and there is no stable shape to which it can evolve through a progression of equilibrium forms, except in one case, which was hitherto unsuspected. This is the case of certain drops of equatorial radius large compared with the radius of the support – drops we call obese. At its critical angular velocity an obese drop loses stability to a fully three-dimensional, C-shaped form that is stable and evolves into further, stable C-shaped forms at higher angular velocities up to some limit. Hence the C-shape should be observable in experiments.

Axisymmetric captive drops, whether cylindrical, depleted and skinny, or swollen and obese, are found to lose stability in one of two ways: the initially stable family of axisymmetric shapes either bifurcates to a new family whose members may or may not have axial symmetry; or it reaches a rotation rate beyond which there are simply no equilibrium shapes infinitesimally different from the last member. Both possibilities have also been predicted in other cases, for example the rupturing of a layer of insulating liquid separating conducting fluids at different electrostatic potentials (Michael *et al.* 1974, 1975).

The results for the perfectly cylindrical drop presented in §4 are singular in an important sense. They predict an endless sequence of shape families bifurcating from the cylinder family (see figure 3). However, if the volume of liquid deviates at all from that of a cylinder, there is a rotation rate beyond which axisymmetric shapes do not exist (see figure 13). Gravity in the axial direction may be expected to have this same effect on the equilibrium shapes of axisymmetric drops. Moreover, because gravity disrupts the symmetry of the drop shape about the equatorial plane, it may cause the supercritical and subcritical bifurcations described here to split into non-intersecting shape families; such bifurcations are called ‘imperfect’ by Thompson & Hunt (1973). An investigation of these possibilities will be the subject of another communication.

Plateau’s (1863) laboratory investigation was the first to shed light on the intricacies of rotating drops. In his experiments a fat drop is immersed in a second, immiscible liquid of lower viscosity and virtually the same density. The drop is penetrated by a slender cylindrical shaft on which is mounted a small disk that is totally surrounded by the drop. Although the drop is held captive on the shaft by surface tension, its wetting lines may be able to move, depending on the wetting properties of the shaft. Thus under some conditions the contact lines may slide freely enough along the shaft to maintain a definite contact angle, rather than remain pinned, which is the boundary condition adopted in the foregoing analysis.

Plateau’s experiments were recently repeated by Tagg & Wang (1978), who confirmed observations made over a century ago. When the shaft with its disk is rapidly spun up from rest to a steady angular velocity that is not too high, the drop takes an axisymmetric form that is the more flattened the greater the steady velocity. However, with successively higher terminal velocities, the drop assumes C-shapes and then two-lobed shapes, in a sequence like that predicted in §6 for the obese captive drop in gyrostatic equilibrium. Whereas the axisymmetric shapes and C-shapes in that sequence are stable, *the two-lobed shapes are not*. Thus two-lobed shapes ought to be seen only as transients.

Plateau’s experiments depart greatly from the ideal of a rigidly rotating liquid drop (Gifford & Scriven 1980). The surrounding immiscible liquid exerts viscous drag on the drop and keeps the liquid within from achieving hydrostatic equilibrium. The flows within and without the drop cause viscous pressure and viscous normal stress on the meniscus that affect its shape and stability. The effects of flows generated during the spin-up can be stronger. Thus more complex, transient drop shapes have been seen (Plateau 1863; Tagg & Wang 1978), including a short-lived toroidal ring of liquid separated from the remainder of the liquid that adheres to the shaft and disk. Some qualitative agreement between experiments like Plateau’s and the theory of captive rotating drops in gyrostatic equilibrium is the best that can be hoped for.

Not even this sort of agreement is always achieved. Carruthers & Grasso (1972 *a, b*) studied the stability of captive rotating liquid cylinders in an experiment like Plateau’s. They found that even short liquid cylinders rotating in an outer liquid of equal density become unstable to a wavy, axisymmetric (r.a., $n = 2$) mode of instability, not the C-mode predicted in §4 (see especially

figure 7) and observed in small-scale, Earthbound experiments in which air is the fluid surrounding the rotating liquid (Fowle *et al.* 1976). Evidently viscous drag between the inner and outer liquids in the experiments of Carruthers & Grasso stabilized the non-gyrostatic states against asymmetric C-mode and two-lobed perturbations until they became unstable to (r.a. $n = 2$) axisymmetric perturbations.

There is an important aspect of the theoretical results in §6 which has no parallel in previous analyses of equilibrium shapes of menisci. The axisymmetric, obese captive drops in losing stability to the fully three-dimensional, stable C-shaped drops obey the often-quoted 'principle of exchange of stabilities'. This rule holds that only if the first shape family that bifurcates from the axisymmetric shapes does so supercritically (i.e. to values of the rotational Bond number, Σ , higher than the value at the bifurcation point), are the shapes of the new family stable and those of the axisymmetric family unstable beyond, i.e. at the higher values of Σ . And indeed, the axisymmetric, obese captive drops do exchange stability in this way with the C-shaped captive drops.

An exchange of stability is known to take place between the family of spheroidal and the bifurcating family of ellipsoidal liquid masses that rotate rigidly and are held together by self-gravitation rather than surface tension (cf. Lyttleton; 1953 Chandrasekhar 1969). Plateau (1863), Appell (1932) and Chandrasekhar (1965) have speculated that entirely free liquid drops which are held together by surface tension and are rotating rigidly may have ellipsoid-like, stable equilibrium shapes that bifurcated from the family of axisymmetric shapes. It was on the basis of such a hypothesis that Plateau (1863) designed his experiments on centimetre-sized, nearly neutrally-buoyant liquid drops as models of much larger-scale, self-gravitating liquid masses. The shapes, stability and bifurcation of freely rotating liquid drops held together by surface tension we have analysed by the finite element algorithm presented in §5. The results are the subject of another communication (Brown & Scriven 1979).

This research was supported by the Fund for Independent Research of the U.S. National Aeronautics and Space Administration, the Graduate School of the University of Minnesota, and the University of Minnesota Computer Center. The authors are grateful to P. Concus and G. H. Golub for valuable discussion and suggestions of methods, and to S. R. Coriell, J. C. C. Nitsche, and F. M. Orr Jr., for particularly stimulating discussions.

REFERENCES

- Appell, P. F. 1932 *Traite de mécanique rationnelle*, vol. 4, ch. 9. Paris: Gauthier-Villars.
- Bathe, K. J. & Wilson, E. L. 1976 *Numerical methods in finite element analysis*. Englewood Cliffs, New Jersey: Prentice-Hall.
- Brown, R. A. 1979 Finite element methods for the calculation of capillary surfaces, *J. Comp. Phys.* **33**, 217–235.
- Brown, R. A. & Scriven, L. E. 1980 The shape and stability of rotating liquid drops, *Proc. R. Soc. Lond. A* (In the press.)
- Brown, R. A., Orr, F. M. Jr. & Scriven, L. E. 1980 Static drop on an inclined plate: analysis by the finite element method, *J. Colloid Interface Sci.* **73**, 76–87.
- Carruthers, J. R. 1975 Crystal growth from the melt. In *Treatise on solid state chemistry*, vol. 5 (ed. N. B. Hannay). New York: Plenum Press.
- Carruthers, J. R., Gibson, E. G., Klett, M. G., & Facemire, B. R. 1977 Studies for rotating liquid floating zones on Skylab IV. In *Materials sciences in space with application to space processing* (ed. L. Steg). New York: AIAA.
- Carruthers, J. R. & Grasso, M. 1972a Studies of floating zones in simulated zero gravity. *J. appl. Phys.* **43**, 436–445.
- Carruthers, J. R. & Grasso, M. 1972b The stabilities of floating liquid zones in simulated zero gravity. *J. Crystal Growth* **13**, 611–614.

- Carslaw, H. S. & Jaeger, J. C. 1959 *Conduction of heat in solids*, 2nd edn. London: Oxford University Press.
- Chandrasekhar, S. 1965 The stability of a rotating liquid drop. *Proc. R. Soc. Lond. A* **286**, 1–26.
- Chandrasekhar, S. 1969 *Ellipsoidal figures of equilibrium*. New Haven: Yale University Press.
- Coriell, S. R. & Cordes, M. R. 1977 Theory of molten zone shape and stability. *J. Crystal Growth* **42**, 466–472.
- Coriell, S. R., Hardy, S. C. & Cordes, M. R. 1977 Stability of liquid zones. *J. Colloid Interface Sci.* **60**, 126–136.
- Courant, P. & Hilbert, D. 1953 *Methods of mathematical physics*, vol. I. New York: Interscience.
- Finalyson, B. A. 1972 *The method of weighted residuals*. New York: Academic Press.
- Fowle, A. A., Haggarty, J. S., Perron, R. R., Strong, P. F., & Swanson, J. R. 1976 Float-zone processing in a weightless environment. NASA CR-2768. Washington, D.C.: National Aeronautics and Space Administration.
- Gifford, W. A. & Scriven, L. E. 1980 On simulating zero gravity by Plateau's experiment. *J. appl. Phys.*, to be submitted.
- Gillette, R. D. & Dyson, D. C. 1971 Stability of fluid interfaces of revolution between equal solid circular plates. *Chem. Engng J.* **2**, 44–54.
- Golub, G. H. 1973 Some modified matrix eigenvalue problems. *SIAM Rev.* **15**, 318–334.
- Golub, G. H. & Underwood, R. R. 1977 The block-Lanczos method for computing eigenvalues. In *Mathematical software III*. New York: Academic Press.
- Hardy, S. & Coriell, S. R. 1974 Melt shape in weightless crystal growth. In *NBS Space Processing Research*, NBSIR 74-611. U.S. Department of Commerce.
- Howe, W. 1887 Ph.D. Inaugural Dissertation, Friedrich-Wilhelms-Universität, Berlin.
- Huh, C. 1969 Capillary hydrodynamics: interfacial instability and the solid/liquid/fluid contact line. Ph.D. thesis, University of Minnesota, Minneapolis.
- Lamb, H. 1932 *Hydrodynamics* (6th edn), reprinted by Dover Press, New York.
- Laplace, P. S. 1805 Theory of capillary attraction. Supplement to the tenth book of *Celestial Mechanics*, (translated and annotated by N. Bowditch, 1839), 1966 reprint by Chelsea, New York.
- Lyttleton, R. A. 1953 *The stability of rotating liquid masses*. Cambridge University Press.
- Majumdar, S. R. & Michael, D. H. 1976 The equilibrium and stability of two-dimensional pendent drops. *Proc. R. Soc. Lond. A* **351**, 89–115.
- Michael, D. H., Norbury, J. & O'Neill, M. E. 1974 Electrohydrostatic instability in electrically stressed dielectric fluids. Part 1. *J. Fluid Mech.* **66**, 289–308.
- Michael, D. H., Norbury, J. & O'Neill, M. E. 1975 Electrohydrostatic instability in electrically stressed dielectric fluids. Part 2. *J. Fluid Mech.* **72**, 95–112.
- Michael, D. H. & Williams, P. G. 1976 Equilibrium and stability of axisymmetric pendent drops. *Proc. R. Soc. Lond. A* **351**, 117–127.
- Michael, D. H. & Williams, P. G. 1977 The equilibrium and stability of sessile drops. *Proc. R. Soc. Lond. A* **354**, 127–136.
- Millman, M. H. and Keller, J. B. 1969 Perturbation theory of nonlinear boundary-value problems. *J. math. Phys.* **10**, 342–361.
- Moler, C. B. & Stewart, G. W. 1973 An algorithm for generalized matrix eigenvalue problems. *SIAM J. numer. Anal.* **10**, 241–256.
- Orr, F. M. Jr., Scriven, L. E., & Rivas, A. P. 1975 Menisci in arrays of cylinders: numerical simulation by finite elements. *J. Colloid Interface Sci.* **52**, 602–610.
- Pimbley, G. H. Jr. 1976 Stationary solutions of the problem of Rayleigh–Taylor instability. *J. math. Anal. Appl.* **55**, 170–206.
- Pitts, E. 1973 The stability of pendent liquid drops. Part I. Drops formed in a narrow gap. *J. Fluid Mech.* **59**, 753–767.
- Pitts, E. 1974 The stability of pendent liquid drops. Part II. Axial symmetry. *J. Fluid Mech.* **63**, 487–508.
- Pitts, E. 1976 The stability of a drop hanging from a tube. *J. Inst. Math. Appl.* **17**, 387–397.
- Plateau, J. 1863 Experimental and theoretical researches on the figures of equilibrium of a liquid mass withdrawn from the action of gravity. In *Annual Report of the Board of Regents of the Smithsonian Institution*, pp. 270–285. Washington, D.C.
- Rayleigh, Lord 1879 On the instability of jets. *Proc. Lond. math. Soc.* **10**, 4–13.
- Strang, G. & Fix, G. J. 1973 *An analysis of the finite element method*. Englewood Cliffs, New Jersey: Prentice-Hall.
- Tagg, R. A. & Wang, T. G. 1978 The shapes of rotating liquid drops neutrally buoyant in another liquid. *Bull. Am. phys. Soc.* **23**, 1006.
- Thompson, J. M. T. & Hunt, G. W. 1973 *A general theory of elastic stability*. New York: John Wiley & Sons.
- Thompson, J. M. T. & Hunt, G. W. 1975 Towards a unified bifurcation theory. *Z. angew. Math. Phys.* **26**, 581–603.
- Underwood, R. R. 1975 An iterative block-Lanczos method for the solution of large sparse symmetric eigenproblems. Ph.D. thesis, Stanford University.
- Wilkinson, J. H. 1965 *The algebraic eigenvalue problem*. Oxford: Clarendon Press.
- Young, T. 1805 Essay on the cohesion of fluids, *Phil. Trans. R. Soc. Lond.* **95**, 68–86.